 FDMP, vol.10, no.2, pp.197-240, 2014

The JEREMI-Project on Thermocapillary Convection in Liquid Bridges. Part B: Overview on Impact of Co-axial Gas Flow.

V. Shevtsova[1], Y. Gaponenko[1], H.C. Kuhlmann[2], M. Lappa[3], M. Lukasser[2], S. Matsumoto[4], A. Mialdun[1], J.M. Montanero[5], K. Nishino[6] and I. Ueno[7]

Abstract: Pure surface-tension-driven flow is a unique type of flow that can be controlled through external manipulation of thermal and/or mechanical boundary conditions at the free liquid surface where the entire driving force for the convection is generated. This unique feature has been exploited in recent studies for the active control of the flow instability. The use of forced coaxial gas streams has been proposed as a way to stabilize the Marangoni convection in liquid bridges in the planned space experiment JEREMI (Japanese and European Research Experiment on Marangoni Instabilities). It is aimed at understanding the mechanism of the instability and the role of the surface heat transfer and surface shear stresses. This overview presents corresponding preparatory experimental and numerical studies.

1 Introduction

In the early days of spaceflight, it was believed that crystals of exceptional quality could be grown from the melt in the microgravity environment due to the absence of the undesired buoyant convection. However, first space-based experiments performed independently by D. Schwabe and C.H. Chun at the same missions (TEXUS 3a 1980, partly successful) and (TEXUS 3b 1981, fully successful) showed that thermocapillary forces provide a very strong natural-convection mechanism under microgravity conditions (Chun and Schwabe, 1982; Schwabe, 2014). Over the time the system of a thermocapillary liquid bridge became a standard setup for the study

[1] University of Brussels (ULB), Belgium.
[2] Vienna University of Technology, Vienna, Austria.
[3] Telespazio, Naples, Italy.
[4] JAXA, Tsukuba, Japan.
[5] University of Extremadura, Spain.
[6] Yokohama National University, Yokohama, Japan.
[7] Tokyo University of Science, Chiba.

of thermocapillary flows (Schwabe, Preisser, and Scharmann, 1982; Kuhlmann, 1999; Lappa, 2010, 2012b).

Under typical ground conditions, the natural convection around the liquid bridge is relatively weak, so its effect has been neglected in the past. This led to relatively large uncertainties in the determination of, e.g., the critical Marangoni number for the onset of a three-dimensional flow (Shevtsova, Mialdun, Ueno, Kawamura, Nishino, and Lappa, 2011). Experimental evidence of the important role of heat transport through liquid-gas interface in the stability of the thermocapillary flow in LB has been reported since the 80s. Dressler and Sivakumaran (1988) performed experiments on a silicone-oil liquid bridge using a vertical jet of air blown tangentially over the free surface for producing a viscous shear force opposing the Marangoni shear stresses on the free surface.

The Japanese–European Research Experiment on Marangoni Instability (JEREMI) consortium is preparing a space experiment on the ISS with a launch date of 2016 in which the ambient atmosphere is much better defined. This may be achieved by placing a liquid bridge into a coaxial gas flow in the annular space around the liquid bridge. Of particular interest is the control of the threshold of an oscillatory flow in the liquid zone by the temperature and velocity fields in the ambient gas. For large-Prandtl-number liquids, particularly the 5cSt silicone oil which will be used, the instability arises in form of hydrothermal waves (Smith and Davis, 1983; Wanschura, Shevtsova, Kuhlmann, and Rath, 1995; Leypoldt, Kuhlmann, and Rath, 2000). The JEREMI experiment is being developed by the International Topical Team on *Marangoni instabilities in systems with cylindrical symmetry* and is supported on the European side in the framework of the ESA project IAO-2004-097 *Thermocapillary oscillatory motion and interfacial heat exchange*.

In addition to controlling the flow in thermocapillary liquid bridges, the JEREMI experiment provides the opportunity to study particle accumulation structures (PAS). Research on PAS is supported by ESA in the framework of the project IAO-2000-091 *Dynamics of suspended particles in periodic vortex flows* and has been the subject of part A of this series of two overview papers (Kuhlmann, Lappa, Melnikov, Mukin, Muldoon, Pushkin, Shevtsova, and Ueno, 2014).

The present part B covers the subject of thermocapillary-flow control by a coaxial gas flow and the related preparations of the JEREMI experiment. The forced gas flow along the interface provides two actions: shear stress and heat exchange. Even in the case of a passive ambient gas (no forced flow), the experiments by Shevtsova, Mialdun, and Mojahed (2005), Mialdun and Shevtsova (2006) on free liquid bridges and on liquid bridges protected by a coaxial cylindrical shield tube (with temperature control of the shield tube), respectively, clearly showed a dependence of the critical temperature difference and the critical frequency of oscillation on

the surrounding conditions and the temperature of shielding. Kamotani's group has performed experiments (Kamotani, Wang, Hatta, Wang, and Yoda, 2003; Wang, Kamotani, and Yoda, 2007) placing a liquid bridge in an oven at different temperatures demonstrating a strong dependence of the critical parameters on the temperature of the ambient air. In some of their experiments (Kamotani, Wang, Hatta, Wang, and Yoda, 2003) a thin plastic plate with a circular hole was placed horizontally around a liquid column at a certain height without touching the free surface in order to suppress convection in the ambient air. Depending on the axial location of the plate the stability of the flow varied strongly due to the alteration of the heat transfer near the free surface. Irikura, Arakawa, Ueno, and Kawamura (2005) and Kousaka and Kawamura (2006) experimentally and numerically investigated the way in which the volume of gas space around a liquid bridge affects the onset of its instability. The volume of the ambient air region was varied by placing two thin disks perpendicular to the liquid bridge. Similar configurations were studied numerically and experimentally by Tiwari and Nishino (2007, 2010).

The study of the dynamic behavior of liquid bridges in response to a coaxial gas flow began with the analysis of isothermal cases. Gaponenko, Ryzhkov, and Shevtsova (2010); Gaponenko, Glockner, Mialdun, and Shevtsova (2011); Gaponenko, Mialdun, and Shevtsova (2012) and Herrada, López-Herrera, Vega, and Montanero (2011) have recently examined isothermal gas–liquid flows in an annulus. The first three studies were focused on the characteristics of the liquid flow driven by gas, and the last one on the interface deformation. Along with geometrical scales the key parameters responsible for flow dynamics are the inlet gas velocity and the viscosity ratio between the two phases. The surface tension plays an important role for the static and dynamic (flow-induced) deformations of the interface. Dynamic free-surface deformations caused by a shear-driven flow were experimentally studied by Matsunaga, Mialdun, Nishino, and Shevtsova (2012) in a liquid bridge of 5cSt silicone oil. As a general trend, the flow-induced deformation grows with the gas velocity. It also displays a strong dependence on the liquid volume ratio and the orientation of the gas stream parallel or anti-parallel to the interface flow. All experimental and numerical results in the above mentioned studies on the magnitude of the dynamic free-surface deformation for the volume ratio $\mathscr{V} = 1$ are in an excellent agreement and cover 1–10 μm. The study was limited to a gas velocity up 2m/s (or $Re^g < 560$).

Only a few studies have been concerned with both the flow in a non-isothermal liquid bridge and in the surrounding gas. Experiments in a 2cSt-silicone-oil/air system by Ueno, Kawazoe, and Enomoto (2010) showed that the stability of the thermocapillary flow in a liquid bridge is strongly affected by the orientation of the gas stream, even though the gas was at room temperature and the velocity was

rather low, $Re^g \leq 100$. For the geometry considered the steady flow was stabilized when the net gas flow was oriented parallel to thermocapillary-driven flow on the interface, whereas the steady basic flow was destabilized when the net gas flow was oriented in opposite direction to the thermocapillary-driven flow on the interface.

The thermocapillary flow in an infinitely long, non-deformable liquid bridge surrounded by an annular channel of gas with an axial temperature gradient was investigated by Ryzhkov and Shevtsova (2012) using linear–stability analysis (LSA). The authors reported that a net gas flow in the same direction as the thermocapillary surface flow acts destabilizing on the axisymmetric basic flow. A net gas motion in the opposite direction can be stabilizing or destabilizing depending on the gas-flow rate. The different trends for the liquid flow stability with respect to the gas direction between the experiments on finite-length liquid bridges of Ueno, Kawazoe, and Enomoto (2010) and the linear-stability analysis for an infinitely long liquid zone can be attributed to the different axial temperature profiles in gas phase, which was assumed to be linear in the LSA. As a consequence there is no heat exchange between the liquid and the gas in the basic axisymmetric flow state. It occurs only on the level of perturbations. For that reason a cooling or heating of the liquid through the interface by an ambient gas flow cannot be described in the framework of the simple model employed.

Yura, Maruyama, and Nishino (2009) have experimentally studied the effect of a co-axial gas flow on the flow stability in liquid bridges of different volume ratios. The critical temperature difference as a function of the volume ratio consists of two branches with a peaked maximum at a volume roughly corresponding to a straight cylindrical interface. The author reported a shift of the peak to the smaller or larger volume ratios depending on the gas-flow direction. The peak was shifted to the side of smaller volumes $\mathscr{V}$ when the gas flow was opposite to the thermocapillary-driven flow on the interface and to the side of larger volumes $\mathscr{V}$ when the gas flow is co-directed with surface flow. The larger the gas velocity the larger is the shift of the peak.

A comprehensive numerical analysis of the axisymmetric thermocapillary convection in a liquid bridge Pr=12 (n-decane) and Pr=68 (5 cSt silicone oil) in the axisymmetric case was presented by Shevtsova, Gaponenko, and Nepomnyashchy (2013) when the interface is subjected to an axial gas stream. In the case when the gas stream comes from the cold side (anti-parallel to the surface flow), a new oscillatory instability was found in form of an axially travelling wave propagating from the hot to the cold end of the liquid bridge.

2 Microgravity experiment

Microgravity experiments are planned to be conducted in the Fluid Physics Experiment Facility (FPEF) installed in the JEM (KIBO) module on the ISS. The thermocapillary flows in the liquid bridge have been examined in the ground-based experiment only with small liquid bridges, a diameter of 5mm or less. A ground-based experiment with a larger liquid bridge is not feasible because of the limitations caused by buoyant flow, the gravity-induced deformation of the liquid bridge and the difficulty in the formation of large liquid bridges. The effect of the buoyant flow can be represented by the dynamic Bond number, Bd, and the effect of the gravity on the deformation can be represented by the static Bond number, Bo,

$$Bd = (\rho^l - \rho^g) g \beta d / \gamma, \qquad Bo = (\rho^l - \rho^g) g d^2 / \sigma. \tag{1}$$

where ρ is the density of liquid (l) and gas (g), g is the gravitational acceleration, β is the temperature coefficient of volume expansion, d is the characteristic length, σ is the surface tension and $\gamma = -d\sigma/dT$. As indicated by these Bond numbers, the effect of gravity can be neglected either by limiting the size of the liquid bridge to several millimeters or by performing experiments in space. The fact that the objectives of this research can be fulfilled by changing the size of liquid bridge in the diameter range from 10 to 20 mm requires long-term microgravity environments. The International Space Station provides such a long-duration microgravity environment.

2.1 Relevance of the microgravity experiment

The relevance of microgravity experiment in the liquid bridge can be summarized as follows:

- Elimination of buoyancy. The buoyancy force acts in the liquid bridge and in the non-isothermal ambient atmosphere.
- Extension of the accessible aspect-ratio range. On the ground, the accessibly range of length-to-radius ratio is limited by the hydrostatic instability of the liquid bridge.
- Realization of wide range of the Marangoni number Ma. By larger liquid bridges high Marangoni numbers can be realized even with relatively small temperature differences.
- Prevention of hydrostatic interface deformations.
- Enabling the use of low-surface-tension liquids. Microgravity allows to use low-surface-tension liquids which would yield mechanically unstable liquid bridges under terrestrial gravity.
- Accessibility of a wide range of particle sizes. On the ground particles denser

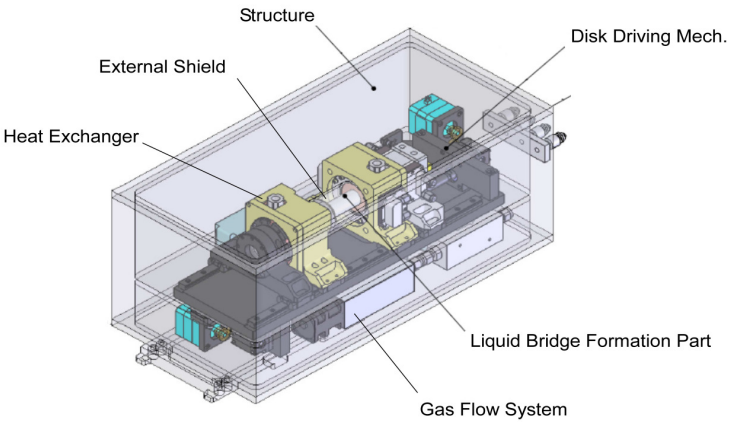

Figure 1: Sketch of the experimental cell

than liquid would rapidly sediment.

- Accessibility of a wider range of Prandtl numbers. On the ground the maximum temperature difference that can be imposed is limited by the melting point and the evaporation rate (boiling point) of the liquid.
- Exploration of the limits of PAS formation. The possibility to create much longer liquid bridges than on the ground allows for a study of particle accumulation as a function of the aspect ratio also for long liquid bridges.
- Utilization of a very long duration of the microgravity environment on the ISS.

2.2 Conceptual design (S. Matsumoto)

The sketch of the experimental cartridge, which will be inserted in the Fluid Physics Experiment Facility (FPEF) is shown in Fig. 1. The cartridge comprises the following parts:
(1) Liquid bridge formation
(2) Temperature control of the end walls bounding the liquid bridge
(3) Ambient gas velocity and temperature control
(4) Observation (video images and temperature measurement)

A pair of rods sustain the liquid bridge. One rod is heated by a resistance heater and other rod cooled by a Peltier device to induce thermocapillary convection in liquid bridge. The liquid-bridge formation part is covered with a cylindrical tube (external shield) made of transparent 3 mm thick polycarbonate in order to supply the controlled flow of gas around the liquid bridge. The gas-flow system generates a forced flow and provides the measurement of the gas velocity. The temperature of the gas is controlled at the heat exchanger just before entering the annular air

gap around the liquid bridge. Three video cameras are used to observe the liquid-bridge shape and the flow field. One takes a video from the top and the other two cameras provide side views of the liquid bridge. Several temperature sensors (thermocouples and thermistors) are equipped to measure the temperature of the inside of the liquid bridge and in the ambient gas. The working fluid will be 5-cSt-silicone oil. Gold-coated acrylic particles will be dispersed into the silicone oil to visualize the flow motion.

3 Mathematical formulation

The mathematical model assumes incompressibility of liquid and gas, linear dependence of surface tension and density on temperature, with all other thermophysical properties of fluids being taken as constant. The physical problem investigated is that of a cylindrical liquid bridge concentrically surrounded by an annular gas channel under conditions of zero gravity. The problem will be formulated in the cylindrical coordinate system (r, φ, z), although some teams use the Cartesian coordinate system in calculations. The geometry of the system and notation are shown in Fig. 2.

The outer cylinder is a solid tube of radius R_{out}. The inner cylinder consists of two solid rods of radius R_0 and a liquid bridge between them, which is kept in its position by surface tension force. Gas of a constant flow rate Q_{in} enters from the right or left and flows through the annular duct of a size $(R_{out} - R_0)$. Moving along the solid rod of the length H_c (H_h) the gas reaches the liquid zone and a forced gas flow interplays with a liquid thermocapillary flow, which is present when the temperature difference is imposed between the rods. After passing the liquid zone of the length d, the gas continues to move through the annular duct over the distance H_h (H_c) up to the tube outlet. The total length of the tube is $L = H_c + H_h + d$. The system of two coaxial cylinders is shown in Fig. 2 in horizontal position which corresponds to the microgravity case. For discussion of the experiments in terrestrial conditions the same notations will be used, while the gravity vector is directed parallel to the axes of cylinder.

When the solid rods, which should have an excellent thermal conductivity, are heated at T_h and cooled at T_c, respectively, with a temperature difference $\Delta T = T_h - T_c$, the temperature variation along the liquid–gas interface drives a significant fluid motion via the thermocapillary effect. At small temperature differences the flow is axisymmetric. With the increase of the temperature difference the flow becomes three-dimensional and the axisymmetry is broken (Wanschura, Shevtsova, Kuhlmann, and Rath, 1995). For a Prandtl number larger than about one, this symmetry-breaking bifurcation leads to an oscillatory flow. Further increase of ΔT leads to co-existence of multiple modes (Shevtsova, D., and Legros, 2003), or ape-

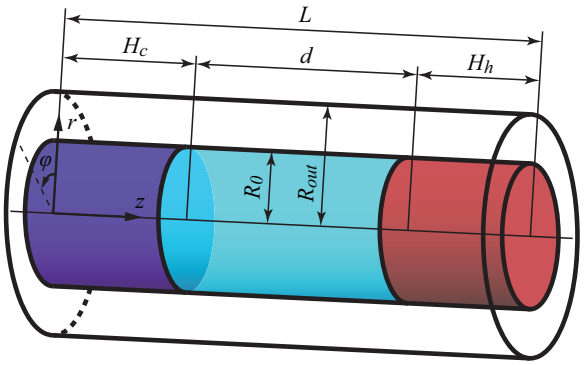

Figure 2: Geometry of the problem

riodicity of the flow (Frank and Schwabe, 1997; Melnikov, Shevtsova, and Legros, 2004). The presence of a gas flow essentially modifies the critical parameters as well as the type of a hydrothermal wave.

3.1 Governing equations

The liquid and gas are considered as Newtonian fluids with temperature-dependent properties. The density ρ, surface tension σ are temperature dependent quantities and to first order they can be expanded in Taylor series.

$$\sigma = \sigma_0 - \gamma(T - T_0) + O(T - T_0)^2, \tag{2}$$

$$\rho^l = \rho_0^l \left[1 - \beta^l (T - T_0)\right] + O(T - T_0)^2, \tag{3}$$

$$\rho^g = \rho_0^g \left[1 - \beta^g (T - T_0)\right] + O(T - T_0)^2, \tag{4}$$

where $T_0 = (T_h + T_c)/2$ is the arithmetic mean temperature of the rods, γ is the surface-tension coefficient, β is the thermal expansion coefficient. The reference quantities σ_0, ρ_0 and ν_0 are evaluated at the mean temperature T_0. The superscripts "l" and "g" relate to the liquid and gas phase, respectively. The variation of the surface tension γ is essential, as it is one of the driving forces of the flow in two-phase system and it appears in the boundary conditions. In terrestrial environment, thermal expansion is treated in the framework of the Boussinesq approximation such that density variations are only taken into account in the buoyancy body-force term.

The dynamics of the system in the geometry of Fig. 2 is described by the momentum, continuity and heat transfer equations for incompressible Newtonian fluids

which are written for gas and liquid:

$$\partial_t \vec{V}^g + (\vec{V}^g \cdot \nabla)\vec{V}^g = -\frac{1}{\rho^g}\nabla P^g + \frac{\mu^g}{\rho^g}\nabla^2 \vec{V}^g + \vec{g}, \tag{5}$$

$$\nabla \cdot \vec{V}^g = 0, \tag{6}$$

$$\partial_t T^g + \vec{V}^g \cdot \nabla T^g = \chi^g \nabla^2 T^g, \tag{7}$$

$$\partial_t \vec{V}^l + (\vec{V}^l \cdot \nabla)\vec{V}^l = -\frac{1}{\rho^l}\nabla P^l + \frac{\mu^l}{\rho^l}\nabla^2 \vec{V}^l + \vec{g}, \tag{8}$$

$$\nabla \cdot \vec{V}^l = 0, \tag{9}$$

$$\partial_t T^l + \vec{V}^l \cdot \nabla T^l = \chi^l \nabla^2 T^l, \tag{10}$$

where $\vec{V}$ and p denote the velocity and pressure fields, T is the temperature; μ is the dynamic viscosity; χ is the thermal diffusivity and $\vec{g}$ is the gravity vector.

3.2 Boundary conditions

Below we discuss boundary conditions of the two-phase flow system with an inlet and outlet. In accordance with the governing equations the boundary conditions are written in dimensional quantities and in the cylindrical coordinate system (r, φ, z).

1) On the plane ends of the rigid rods which are in contact with liquid as well as on the lateral surfaces of the rods which are in contact with gas, we assume no-slip and no-penetration boundary conditions and imposed temperatures.

$$\vec{V}^l(z = H_c) = \vec{V}^l(z = H_h) = 0, \qquad \text{when} \quad 0 \le r \le R_0; \tag{11}$$

$$T(z = H_c) = T_c, \quad T(z = H_h) = T_h, \quad \text{when} \quad 0 \le r \le R_0; \tag{12}$$

$$\vec{V}^g(r = R_0) = 0 \quad \text{when} \quad 0 \le z \le H_c; \quad H_c + d \le z \le L; \tag{13}$$

$$T(r = R_0) = T_c \quad \text{when} \quad 0 \le z \le H_c; \tag{14}$$

$$T(r = R_0) = T_h \quad \text{when} \quad H_c + d \le z \le L; \tag{15}$$

2) No-slip conditions are imposed on the wall of the external tube at $r = R_{out}$; in numerical simulations the tube is kept either at constant temperature T^* or thermally insulated:

$$r = R_{out}, \quad 0 \le z \le L : \ \vec{V}^g = 0. \tag{16}$$

$$T^g = T^* \quad \text{or} \quad \partial_n T = 0 \tag{17}$$

3) Introducing the notation for the gas/liquid interface $h = r(z, \varphi, t)$ the following boundary conditions are adopted:

(a) With the normal vector $\vec{n}$ directed out of the liquid, the boundary condition on the free surface between the viscous fluid and the inviscid gas can be written as

$$[P_l - P_g]\,\mathbf{n}_i - \left(\mathbf{S}^l_{ik}\mathbf{n}_k - \mathbf{S}^g_{ik}\mathbf{n}_k\right) = -[\sigma(\nabla\cdot\mathbf{n})]\,\mathbf{n}_i - \boldsymbol{\tau}_\mathbf{i}\cdot\nabla\sigma \tag{18}$$

here $\mathbf{S}_{ik} = \mathbf{S} = \eta(\partial V_i/\partial x_k + \partial V_k/\partial x_i)$ is the viscous stress tensor. The tangential projections of Eq. (18) define the driving thermocapillary force

$$\tau\cdot\mathbf{S}^l\cdot\mathbf{n} - \tau\cdot\mathbf{S}^g\cdot\mathbf{n} = -\frac{\partial\sigma}{\partial\tau} \tag{19}$$

The normal projection defines the shape of interface,

$$[P_l - P_g] - \left(\mathbf{n}\cdot\mathbf{S}^l\cdot\mathbf{n} - \mathbf{n}\cdot\mathbf{S}^g\cdot\mathbf{n}\right) = -\sigma(\nabla\cdot\mathbf{n}) \tag{20}$$

here $\sigma(\nabla\cdot\mathbf{n}) = \sigma\left(\frac{1}{R_1} + \frac{1}{R_2}\right)$ is the Laplace pressure where R_1 and R_2 are the principal radii of interface curvature. In the absence of flow Eq. (20) reduces to the well known Young-Laplace equation which determine the static shape of a liquid bridge.

A cylinder of motionless liquid, longer than its circumference is unstable, i.e. liquid bridges with aspect ratio $\Gamma \geq 2\pi$. This limit, called the Plateau–Rayleigh stability limit, can be understood in terms of small axisymmetric disturbances that preserve volume. For short bridges, disturbances in azimuthal direction dominate those in radial one. For long bridges, the reverse is true. The presence of a flow either within or outside the cylinder can influence the pressure distribution and the flow stability. There exist experimental studies by Lowry and Steen (1997); Uguz, Alvarez, and Narayanan (2010) considering the behavior of an isothermal liquid bridge surrounded by co-axial flow of a immiscible fluid. In both studies, the focus was made on enhancing the stability of a near-cylindrical liquid bridge approaching the Plateau–Rayleigh limit by using the interplay between density imbalance and flow. The JEREMI experiment may verify the elongation of the length of a liquid bridge beyond the Plateau–Rayleigh limit using stabilization by parallel gas flow although it is yet fixed.

(b) Tangential velocities of liquid and gas are equal; the temperatures of liquid and gas are equal.

$$V^l_\tau = V^g_\tau, \qquad T^l = T^g; \tag{21}$$

(c) The kinematic condition at the interface $r = h(z, \varphi)$ provides

$$V_r = \frac{\partial h}{\partial t} + \frac{\partial h}{\partial z} V_z + \frac{1}{h} \frac{\partial h}{\partial \varphi} V_\varphi \tag{22}$$

Typically, the dynamic deformations caused by the flow of liquid and gas are very small (Montanero, Ferrera, and Shevtsova, 2008; Matsunaga, Mialdun, Nishino, and Shevtsova, 2012) and can be neglected. Thus, the hydrostatic liquid bridge form provides a good approximation of the surface shape. In this approach

$$V_r = 0. \tag{23}$$

(d) The energy conservation at the interface implies a balance between the heat fluxes in both phases

$$k^l \, \vec{n} \cdot \nabla T^l = k^g \, \vec{n} \cdot \nabla T^g, \tag{24}$$

4) At the inlet at $z = 0$ (or $z = L$) the flow is unidirectional and only the axial velocity is non-zero. It has either a parabolic profile or constant value. Alternatively, a constant flow rate, Q_{in} can be used as boundary condition. The temperature of the gas is a parameter of the problem or is equal to the rod temperature.

$$U_z^g = F(r), \quad U_r^g = U_\varphi^g = 0, \quad T^g = T_{in}, \quad R_0 < r < R_{out} \tag{25}$$

5) The flow velocity and pressure at the outlet are not known prior to the solution of the flow problem. The "soft" conditions are applied at outflow boundaries when the velocity profiles are physically appropriate for fully-developed flows, i.e. the velocity profiles are unchanging in the flow direction:

$$\frac{\partial U_z^g}{\partial z} = \frac{\partial U_r^g}{\partial z} = \frac{\partial U_\varphi^g}{\partial z} = 0, \quad \frac{\partial T^g}{\partial z} = 0. \tag{26}$$

The question of whether these conditions allow perturbations to penetrate back inside the tube have been investigated previously by Gaponenko, Ryzhkov, and Shevtsova (2010).

The system is multi-parametric; except the Bond numbers introduced in Eq.(1), the control parameter for the shape of the liquid bridge are the aspect ratio Γ, and the relative liquid volume $\mathscr{V}$, and Capillary number Ca, relevant to dynamic deformations. The additional geometrical parameter Γ_R is the aspect ratio in radial direction.

$$\Gamma = \frac{d}{R_0}, \quad \mathscr{V} = \frac{Vol}{\pi R_0^2 d}, \quad Ca = \frac{\rho \nu^2}{\sigma_0 d}, \quad \Gamma_R = \frac{R_{out}}{R_0}. \tag{27}$$

Here the capillary number Ca is defined as the ratio of viscous force per unit of area to the capillary pressure as it fits to the deformations caused by a thermocapillary flow and by shear stress. There exists another definition of the Capillary number as the ratio of the hydrodynamic pressure to capillary pressure, $C = \gamma \Delta T / \sigma_0$.

The major parameters controlling the flow are: Prandtl number Pr, Grashof number Gr, Reynolds number of the gas Re, Marangoni number Ma, viscosity ratio $\tilde{\mu}$, thermal conductivity ratio $\tilde{k}$

$$Pr = \frac{\mu}{\rho \chi}, \quad Gr = \frac{\beta \Delta T g d^3}{\nu^2}, \quad Re^g = \frac{\rho^g U_0^g D_h}{\mu^g}, \quad Ma = \frac{\gamma \Delta T d}{\mu^l \chi^l}, \quad \tilde{\mu} = \frac{\mu^l}{\mu^g}, \quad \tilde{k} = \frac{k^l}{k^g}, \tag{28}$$

here U_0^g is the mean gas velocity at the inlet, $\nu = \mu/\rho$ is the kinematic viscosity and $D_h = 2\,(R_{out} - R_0)$ is the hydraulic diameter which is a typical length scale in an annulus.

4 Results

4.1 *Two-phase flows and oscillatory instability* $m = 0$ *(Y. Gaponenko, V. Shevtsova)*

4.1.1 *No forced gas flow*

Here we present results of non-linear simulations in the liquid and in the ambient gas for the axisymmetric case. Figure 3 shows isolines of stream functions (upper raw) and temperature field (lower raw) in two phases without forced gas motion for various experimental conditions. The difference between plots (a, b, c) in Fig. 3 occurs in the gravity level and in the temperature of the outer tube. The constant temperature is imposed on the external tube. The liquid moves from the hot to the cold side along the interface and entrains the passive gas. To make the gas flow structure visible the levels of streamlines in gas and liquid are very different. The coordinate $z = 0$ is placed at the beginning of liquid zone. The geometry scales are $R_0 = d = 3$ mm, $R_{out} = 7$ mm, $H_c = H_h = 2$ mm.

The gravity produces a large secondary vortex in the gas near the external cold tube, compare Fig. 3a with $Gr^g = 0$ and Fig. 3b with $Gr^g \approx 200$. The velocity in this vortex is very small and does not affect much the temperature field in the area of its location. Our analysis has shown that decrease of the duct width squeezes the secondary vorticity and then it vanishes; for the considered parameters it occurs at $R_{out} = 5$ mm. Gravity also causes an additional vortex in the liquid close to the cold wall ($Gr^l \approx 2.53 \cdot 10^4$ in Fig. 3b, 3c). It leads to the decrease of velocity on the hotter part of the interface.

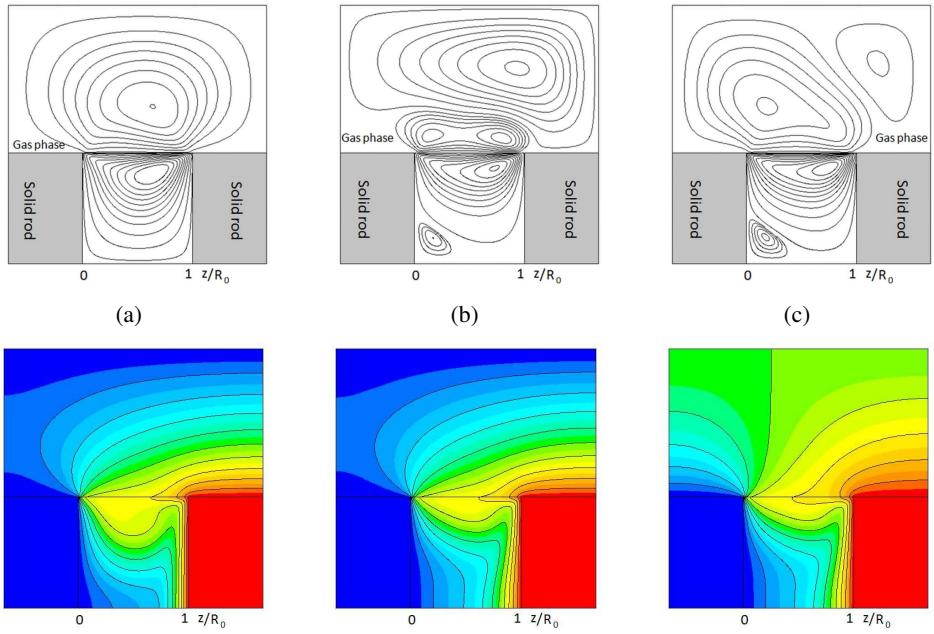

Figure 3: Isolines of stream functions and temperature field in two phases /without forced gas motion, $Pr = 68$, $\Delta T = 10K$, $U_0^g = 0, \Gamma = 1, \Gamma_R = 7/3$. (a) $T(r = R_{out}) = T_c$, $g = 0$; (b) $T(r = R_{out}) = T_c$, $g = g_0$; (c) $T(r = R_{out}) = T_0$, $g = g_0$.

Another important parameter for the gas flow structure is the viscosity ratio between the two phases. In the case of the fluids 5cSt silicone oil/gas, $\mu^l/\mu^g = 255$. The large viscosity ratio causes the sharp gradients of the velocity on both sides of the interface. Our calculations have shown that replacing silicone oil by the acetone ($\mu^l/\mu^g = 17$) the shear driven flow in the gas becomes strong enough to suppress the secondary vortex driven by the gravity.

Changing temperature of the outer wall from T_c to the mean temperature T_0 affects drastically the heat transfer through the interface and the flow structure, see Fig. 3c. Correspondingly, the heat flux through the interface is different from two previous cases, although in all the cases the heat flux is positive and interface is loosing heat. Here we would like to draw attention to the following point: the presence of ambient gas even at the mean temperature, which is natural for any experiment, cools the free surface.

4.1.2 Impact of forced gas flow

The non-steady two-dimensional problem was solved using dimensional variables in two domains for each phase separately with taking into account the boundary conditions at the interface. The problem is analyzed in the absence and presence of gravity. The commercial solver FLUENT v.6.3 was used for solving governing equations Eqs. (2)–(26).

The steady flow was examined for the mean gas temperature at the inlet and at the outer tube. For large viscosity ratio μ^l/μ^g the shear stresses caused by gas are small and the thermal effects plays an important role. The steady temperature distribution in radial direction in both phases at the middle of the liquid zone is shown in Fig. 4a for different direction of the gas flow with respect to the liquid. The temperature inside liquid remains practically the same regardless the gas-flow direction when its velocity is low, $U^g \leq |0.05|$m/s. Outside of the liquid, the gas temperature decreases almost linearly towards the external wall in the case of passive gas, curve 1. When gas enters from the hot side, (curves 2 and 3) its temperature is increasing with respect to the motionless gas. Opposite situation is observed when gas enters from the cold side (curves 4 and 5), the gas temperature decreases. The deviation of the temperature from that of motionless gas grows with the gas velocity and its profile also depends on the length of the solid rods.

Entering the duct, the gas is moving along the hot (cold) rod during the time $\sim H_h/U_0^g$ while the thermal time is δ^2/χ^g, where δ is the length scale of the pre-heated zone in gas in radial direction. Thus, the layer of the gas pre-heated by rods has thickness

$$\delta \sim \sqrt{H\chi^g/U_0^g}$$

For relatively small U_0^g (curves 2 and 3) the gas is heated over the entire duct width, $\delta \sim (R_{out} - R_0)$ and it loses heat being in contact with liquid. With increase of the gas velocity the temperature profile across the duct deviates from linear one. The deviations are much larger when gas enters from cold side. The similar trends were observed in the experiments described below, see Fig. 9 in the section 4.3.

Two-phase simulations allow us to determine the local and average heat fluxes through the interface. The local heat flux $\tilde{q}(z)$ through the free surface area is determined as

$$\tilde{q}(z) = -k^l\,\partial_r T^l_{r=R_0} \qquad \text{and can be scaled as} \qquad \tilde{q}(z) = \frac{k^l \Delta T}{R_0}\,q. \tag{29}$$

where q is dimensionless heat flux. Considering the flow only in liquid phase, the heat flux through the unit of the free surface can be written using the Biot number,

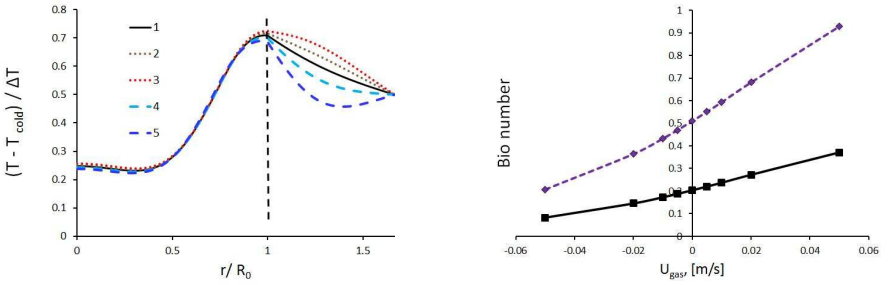

(a) (b)

Figure 4: (a) Temperature profiles in the radial direction in the middle of liquid zone for different gas velocities: curve 1 corresponds to $U^g = 0$; curves 2 and 3 correspond to gas entering from hot side with velocity $U^g = -0.02$ m/s and $U^g = -0.05$ m/s, respectively; curves 4 and 5 correspond to gas entering from the cold side with velocity $U^g = 0.02$ m/s ($Re^g \approx 6$) and $U^g = 0.05$ m/s ($Re^g \approx 14$), respectively; (b) The Biot number as a function of gas velocity calculated via average heat flux through the interface. Other parameters for both graphs are ΔT=15 K and Earth gravity $g = g_0$.

Bi,

$$q_{Bi} = -k^l \, \partial_r T^l_{r=R_0} = h(T_s - T_{amb}) \quad \text{or} \quad q_{Bi} = Bi \left(\frac{k^l}{R_0} \right) (T_s - T_{amb}), \quad Bi = \frac{h R_0}{k^l}.$$

The net flux though interface is determined as $Q = 2\pi R_0 \int q(z) dz$. The equality of the flux Q calculated via Eq. (29) and via q_{Bi} provides relations for determination of the Biot number from two-phase calculations

$$Bi = \frac{\Delta T}{\delta T} q, \qquad \text{where} \quad \delta T = < (T_s - T_{amb}) >, \quad q_{av} = \int_0^1 q d[z]. \tag{30}$$

here q_{av} is dimensionless averaged heat flux. There is some uncertainties in this definition related to the choice of T_{amb}, see discussion by Gaponenko and Shevtsova (2012). The variation of Biot number as a function of the gas velocity is shown in Fig. 4b for $\delta T = \Delta T$ (solid curve) and for $\delta T = 0.4\Delta T$ (dashed curve). It provides $Bi \approx 0.2$ (or 0.5) for passive gas $U^g = 0$, decreasing in the case of hot side gas $U^g < 0$ and increasing in the case of cold side gas $U^g > 0$. The heat flux is positive when the liquid locally loses heat and negative for heat gain. Again, these results show the same trend as the experimental ones, presented in Fig. 10 in the section 4.3.

We have found a new oscillatory instability at the critical values of the couple $[\Delta T_{cr}, U^g_{0cr}]$ when the gas is blown from the cold side, (Shevtsova, Gaponenko,

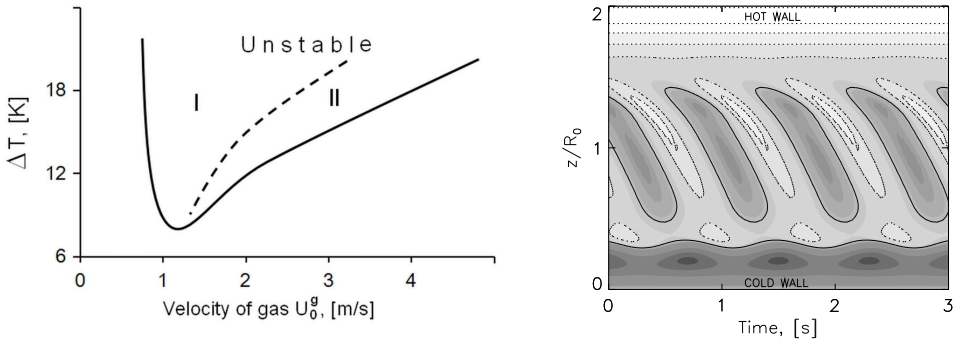

Figure 5: (a) Stability diagramm (ΔT vs U_0^g); (b) Convection cells on the interface as projection of the interface velocity $U_g = 1.5$ m/s, $\Delta T = 12K$. The dotted curves specify the regions with the negative velocity on the free surface.

and Nepomnyashchy, 2013). The stability diagram presented in Fig. 5a displays a limited region of the parameter space where the instability occurs. We assign the appearance of the instability to the interface cooling by the gas with additional action of counter directed shear stresses which decelerate the velocity of the free surface. The instability evolves under the action of three effects: the shear stress diminishing the interface velocity, the radial velocity disturbance tending to shift the temperature disturbance downward, and the plain drift of the disturbance by the net thermocapillary flow. Some similarity can be found with the problem considering inclined temperature gradient in liquid layer of water-air system (Nepomnyashchy, Simanovskii, and Braverman, 2001). The dashed curve in Fig. 5a depict the boundary between two oscillatory regimes when the first (I) is controlled by the Marangoni force and second (II) is controlled by the shear stress.

The convection cells in the oscillatory regime II are shown in Fig. 5b as projection of an interface velocity. In the central part, the large elongated cells (indicating a positive velocity) alternate with the smaller cells (indicating a negative velocity). The dashed curves specify the region with the negative velocity. On the cold side, the small horizontally extended cells designate the presence of the permanent vortex caused by the gas flow and the wavy horizontal curve depicts the location of the zero axial velocity. Accordingly, the uniform colors near the hot wall show the stable position of the vortex caused by the Marangoni flow. Thus, two basic vortices with opposite circulation are attached to the end walls. The large vertical cells also highlight the area of maximal vortex activity, wherein the two other weak vortices appear and fade over time. The convective cells clearly show that traveling wave in the presence of a cold gas flow propagates from the hot to cold end. We attribute the unusual direction of the wave propagation to the inverted radial temperature

distribution in the liquid near the interface, which is developed due to the cooling of the interface by the cold gas flow.

Apparently the thermal effect of the gas is more important than the shear stress provided by gas for high Prandtl numbers. In our opinion the suitable parameter for analysis of the instability is the Péclet number, $Pe = U_0^g(\mu^g/\mu^l)R_0/\chi^l)$, which expresses the relative contribution of advective to thermal diffusive transport. More detailed discussion about role of viscosity ratio can be found in Shevtsova, Gaponenko, and Nepomnyashchy (2013). Presently, the study of two-phase non-linear problem is continued in three-dimensional formulation.

4.2 Flow stability (M. Lukasser and H. C. Kuhlmann)

Correct prediction of the critical onset of hydrothermal waves in thermocapillary liquid bridges is very important for the planned JEREMI experiment, as the *a priori* knowledge of the temperature difference beyond which the flow becomes oscillatory saves a large amount of microgravity-experiment time which would otherwise be consumed to search for the critical point. This is particularly important for larger-size liquid bridges, because the relevant thermal diffusion time increases quadratically with the linear dimension of the liquid volume.

To compute the critical Marangoni numbers and oscillation frequencies a linear stability analysis of the steady basic axisymmetric thermocapillary flow in liquid bridges is carried out. To that end the code MaranStable has been developed. It is based on finite volumes on a non-uniform staggered grid. In a first step the axisymmetric basic flow is calculated. Based on this, the linear stability of the basic flow is calculated using three-dimensional normal modes in the second step. The code is capable of taking into account

1. forced convection and heat transfer in the ambient gas,
2. static liquid–gas interfacial deformations of the liquid bridge,
3. temperature-dependence of the material properties of the liquid and the gas,
4. flow-induced (dynamic) free-surface deformations caused by the steady basic flow.

Of these points the third one has the largest effect on the flow stability, in particular, the variability of the viscosity of the liquid. Variable fluid properties are important when the critical temperature difference is large. Such situations are expected to arise when the outer gas flow and the thermocapillary surface flow of the liquid bridge are oriented in the same direction (co-flow configuration, see below). The

code was extensively verified, by comparison with published results (e.g. by Levenstam, Amberg, and Winkler, 2001) and also with independent computations of Y. Gaponenko (private communication).

The coupling of the flows and the temperature fields in the liquid and the gas phase is demonstrated in figure 6 for the two-dimensional axisymmetric thermocapillary flow for $\mathrm{Pr} = 67$ and $\mathrm{Ma}/\mathrm{Pr} = 362$ using the geometry and the fluids (argon and silicon fluid "KF-96L - 5") as defined in the JEREMI project. The material data were evaluated at the mean temperature. The boundary conditions are in the range of the experimental parameters for a subcritical flow with $\Delta T = 26°\mathrm{C}$. For these parameters a two-dimensional axisymmetric flow is expected. A counter-flow situation is considered in which the gas flow (left to right) is directed opposite to the thermocapillary flow on the free-surface (right to left). From the inlet with a constant radial profile of the axial gas velocity a fully-developed annular channel flow develops. In the vicinity of the free surface very sharp velocity gradients arise owing to the much small kinematic viscosity of the gas as compared to that of the liquid. This is shown in the circular inset for the flow in the gas phase near the free surface and the hot disk axially bounding the liquid bridge. Due to the free-surface flow on the liquid side the axial gas flow is reversed within a very shallow layer at the free surface. The radial gradients of the axial velocity become less near the middle of the free surface and grow larger again near cold wall owing to the sharp peak of the thermocapillary stress on the interface near the cold wall (Kuhlmann, Wanschura, Rath, and Yoda, 2000). As the free-surface jet impinges tangentially on

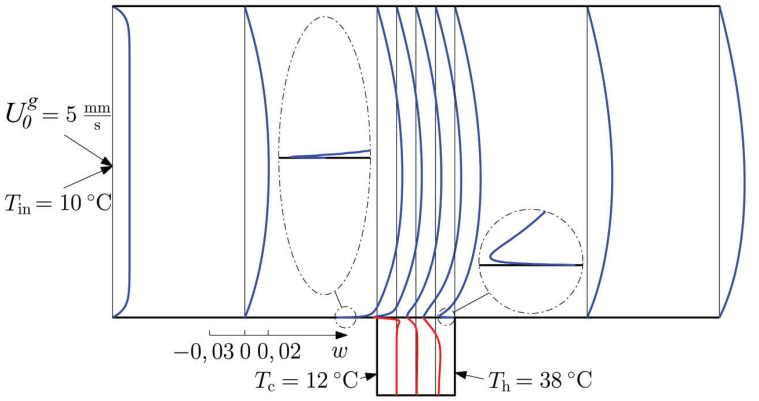

Figure 6: Axial velocity profiles for the combined forced and thermocapillary flow for $\mathrm{Ma}/\mathrm{Pr} = 362$, $\mathrm{Pr} = 67$ shown at axial positions indicated by vertical black lines. Material properties of argon (blue) and silicon fluid "KF-96L - 5" (red) at $T_0 = 25°\mathrm{C}$ were used.

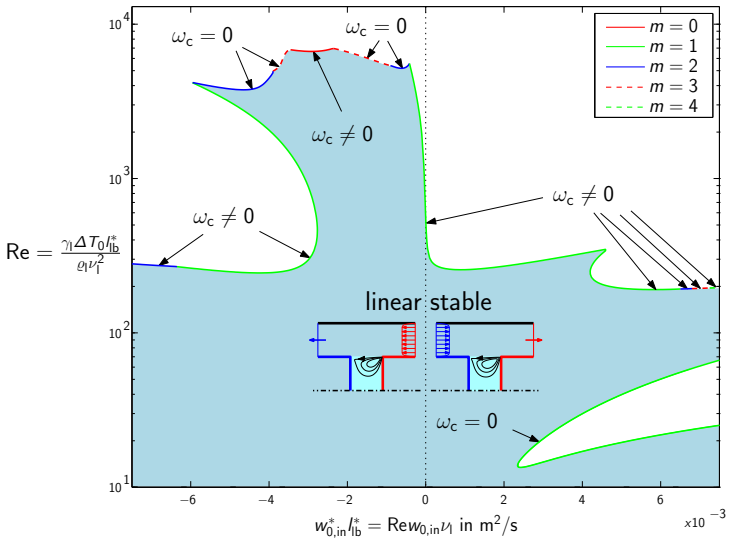

Figure 7: Critical thermocapillary Reynolds number as a function of the mean velocity $w_{0,in}$ in the gas phase. The shaded region is linearly stable.

the cold corner a very thin layer of a reversed gas flow arises on the cold cylindrical wall (large oval inset). These considerations indicate the accuracy requirements to correctly resolve the flow field and the associated large numerical effort.

Turning to the linear flow stability, a typical example for silicon fluid KF-96L-5 and argon at 25°C and 101325 Pa is given in figure 7. For these calculations we assumed a cylindrical liquid volume with a non-deformable free surface and constant material parameters. The critical thermocapillary Reynolds number $\mathrm{Re} = \mathrm{Ma}/\mathrm{Pr}$ is shown as a function of the mean velocity U_0^g in the gas phase. Color indicates the azimuthal wave number m of the critical mode and the type of instability (oscillatory/stationary) is qualitatively indicated by ω_c. For the given parameters ($\Gamma = H_h/d = H_c/d = 1$ and $R_{out}/R_0 = 2$) the critical thermocapillary Reynolds number is very sensitive to the motion in the gas phase as indicated by the steep slope of Re_c for $U_0^g \to 0\,\mathrm{m/s}$. On the scale shown in the figure a slight gas stream co-flowing with the thermocapillary surface flow can (linearly) stabilize the steady basic state by about one order of magnitude of the critical Reynolds number. Moreover, for a stronger co-flow a linearly stable window appears upon an increase of the magnitude of the gas flow. A similar non-unique linear stability boundary arises for counter-flow. Quite generally, the counter-flow configuration is more unstable than the co-flow configuration.

To compare the numerical linear stability data with experimental results obtained

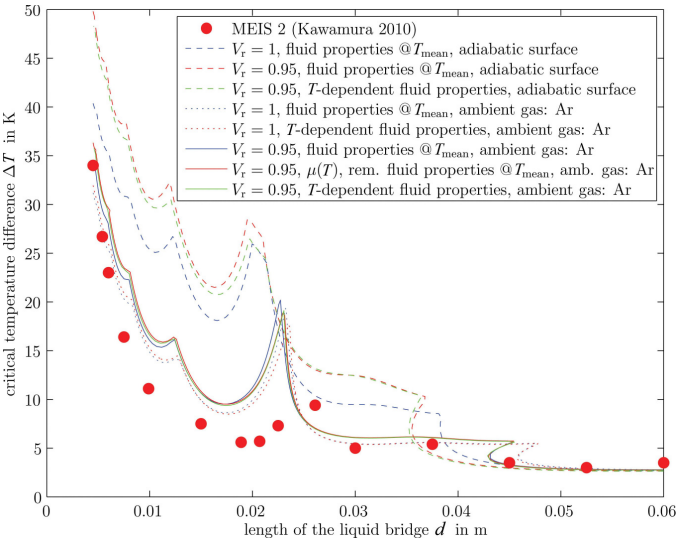

Figure 8: Critical temperature difference as function of the length d of the liquid bridge computed for a model of the space experiment MEIS-II (cf. text). The experimental data of Kawamura, Nishino, Matsumoto, and Ueno (2010) are represented by the dots.

under zero gravity during the space experiment MEIS-II (Kawamura, Nishino, Matsumoto, and Ueno, 2010) the real geometry of the space experiment has been approximated using an annular gas cavity as shown in figure 3 with $R_0 = 0.015\,\mathrm{m}$, $R_{out} = 0.045\,\mathrm{m}$, $H_c = 0.019\,\mathrm{m}$, and $H_h = 0.008\,\mathrm{m}$. The length d was varied. The liquid was 5 cSt silicone oil with nominal Prandtl number of $\mathrm{Pr} = 69$ and the gas was argon. The outer shield and the solid annular disks bounding the gas were maintained at 22°C. The cold cylinder was kept at 20°C while the temperature of the hot cylinder was varied, just as in the space experiment. The effect of different influence factors on the critical temperature difference is explained in figure 8. The model parameter with the largest effect on the stability boundary is the presence of an ambient gas. It can be seen that the basic flow in models with an ambient gas (argon) is less stable than the basic flow in models with an adiabatic free surface (and no ambient gas). The volume ratio V_r is another important parameter which considerably affects the stability. Even a small reduction by 0.05 of the volume ratio leads to a sizable stabilization. The stability boundaries vary little when models with temperature-dependent fluid properties are compared with models whose fluid properties are evaluated at the mean temperature. It must be noted, however, that the temperature differences between the disks are moderate in the case considered. The effect of variable material parameters becomes more pronounced when the

temperature difference increases: Pairwise comparison of the curves for constant and variable material properties (dotted blue with the full red curve, full blue with the full green curve, and dashed green with the full red curve) shows that the critical temperature differences for both cases are very close to each other whenever the temperature difference is small, while there is a remarkable difference between both critical temperature differences when the temperature difference is large.

The critical temperature differences as well as the critical azimuthal wave number (not shown) depend strongly on the length d of the liquid bridge (or aspect ratio Γ). While the shapes of the numerical and experimental stability boundaries agree qualitatively, the quantitative agreement is best for long liquid bridges. The remaining differences can have various reasons. On the numerical side, differences may result from the idealization of the boundary conditions (thermal boundary conditions along the shield and the heater and cooler rods) or uncertainties in the data for the thermo-physical fluid properties. Moreover, neglecting dynamic surface deformations for the perturbation flow might have a small influence. On the experimental side, it is clear that the boundary conditions and, therefore, the basic flow are not axisymmetric. This broken symmetry in the space experiment owing to the asymmetric restriction of the gas phase volume may have an effect on the stability boundaries and could also be the reason for the onset of oscillations at lower temperature differences than predicted numerically for perfectly axisymmetric boundary conditions. If the broken axisymmetry is confirmed to be the primary reason for the deviations of the critical temperature difference, much better experimental onset data can be expected from JEREMI, because of the precisely defined ambient gas conditions and the nearly perfect axisymmetry of the geometry.

4.3 Experimental studies on $\mathrm{Ma_c}$ *at Tokyo University of Science (TUS)*

This study is conducted as a series of ground preparation experiment for the joint project JEREMI (Japan-Europe Research Experiment on Marangoni Instability) that aims at future on-orbit experiments in Kibo, the Japanese Experiment Module, on the International Space Station scheduled for after 2016. One of the main objectives of the JEREMI is to explore the effect of the heat transfer between the liquid bridge and the ambient gas on the critical conditions at which the flow changes from steady two-dimensional to oscillatory three-dimensional. Several experimental investigations have revealed a significant effect of the heat transfer between liquid and gas on the critical Marangoni number $\mathrm{Ma_c}$ (Kamotani, Wang, Hatta, Wang, and Yoda, 2003; Ueno, Kawazoe, and Enomoto, 2010). We have paid attention to the effect of the heat transfer between the liquid bridge and the ambient gas on the critical condition for the half-zone liquid bridge as well as to particle accumulation structures (PAS) (see Kuhlmann, Lappa, Melnikov, Mukin, Muldoon,

Pushkin, Shevtsova, and Ueno, 2014). In order to take into account the effect of the heat transfer between the liquid bridge and the ambient gas, we employ a coaxial shield cylinder to realize a forced upward or downward flow around the liquid bridge at different gas-flow rates.

4.3.1 Analysis of the thermal fields and heat transfer through the interface

The experimental apparatus is the same as presented in Kuhlmann, Lappa, Melnikov, Mukin, Muldoon, Pushkin, Shevtsova, and Ueno (2014). We employ 2-cSt silicone oil (Pr = 28.1 at 25°C) for the liquid bridge and air for the ambient gas as the test fluids. The liquid bridge is sustained between the top and bottom rods of R_0= 2.5 mm in radius. In the series of the experiments on the critical Marangoni number $\mathrm{Ma_c}$ the aspect ratio $\Gamma(= d/R_0)$ is varied from 0.46 to 1.0, where d is the height of the liquid bridge. The external shield made of Pyrex® glass is mounted coaxially to surround the liquid bridge and enable a symmetric forced flow around the liquid bridge. We fix the radius of the external shield at R_{out}=12.5 mm. The thickness of the glass shield is 1.5 mm.

The direction and the flow rate of the ambient gas flow can be varied. The external shield contains a small window made of zinc selenide (ZnSe) in order to detect the surface temperature of the liquid bridge by an infrared (IR) camera through the external shield and ambient gas region. The height, width and thickness of the window are 22 mm, 7 mm and 1.5 mm, respectively. We convinced ourselves that the effect of the partially non-uniformity of the curvature of the internal wall on the flow field in the ambient gas and in the liquid bridge is negligibly small by carrying out of a series of preliminary experiments.

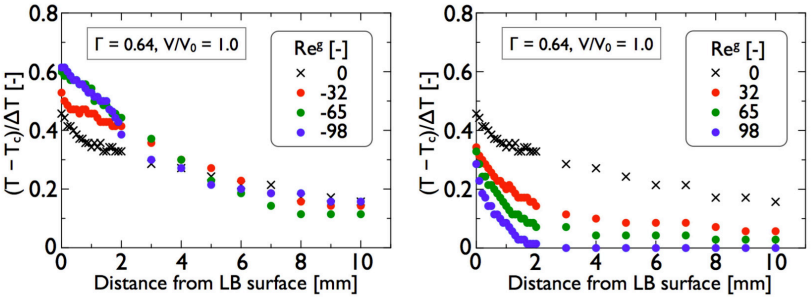

Figure 9: Typical example of the radial distribution of the mean temperature in the ambient gas under $\Gamma = 0.64$ as a function of the Reynolds number for the ambient gas flow $\mathrm{Re^g}$.

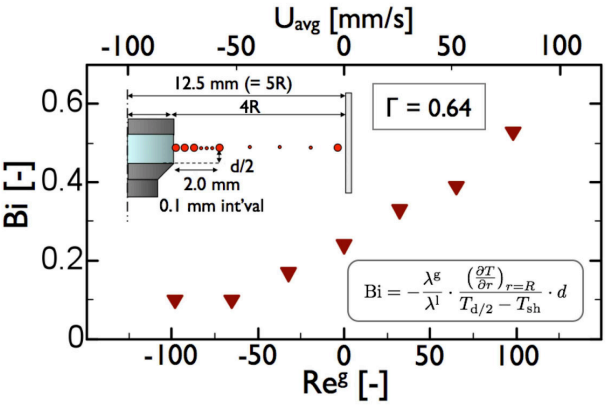

Figure 10: Typical examples for the dependence of the Biot number on the gas-flow Reynolds number Re^{g}. The width of the annular channel through which gas flows is four times larger than the radius of liquid bridge, $R_{out} - R_0 = 4R_0$

The flow in the ambient gas confined by the external shield is characterized by an averaged velocity $U_{\mathrm{avg}} = Q/\pi(R_{\mathrm{out}}^2 - R_0^2)$, where Q is the controlled flow rate in the gas, and the Reynolds number Re^{g}, defined by Eq.(28). Note, that Re^{g} is positive in the case of upward flow, conversely Re^{g} is negative in the case of downward flow. The temperature of the ambient gas is measured by a fine thermocouple at the mid height of the liquid bridge inserted through a tiny hole in the external shield. The thermocouple is traversed from the free surface of the liquid bridge to the inner surface of the shield in steps of 0.1 mm to obtain the radial temperature distribution shown in Fig. 9.

In order to characterize the heat transfer between the liquid bridge and the ambient gas we define the Biot number as

$$\mathrm{Bi} = -\frac{\lambda^{\mathrm{g}}}{\lambda^{l}} \cdot \frac{\left(\frac{\partial T}{\partial r}\right)_{r=R_0}}{T_{(\mathrm{r=R_0,\,z=d/2})} - T_{\mathrm{out}}} \cdot d, \tag{31}$$

where λ^{l} and λ^{g} are the thermal conductivities of the liquid and the ambient gas, respectively, and T_{out} indicates the temperature of the external shield. A typical example of the dependence of the Biot number on Re^{g} is shown in Fig. 10. The behavior of the experimentally determined Biot number as function of Re^{g} is similar to that obtained by two-phase-flow simulations, cf. Fig. 4.

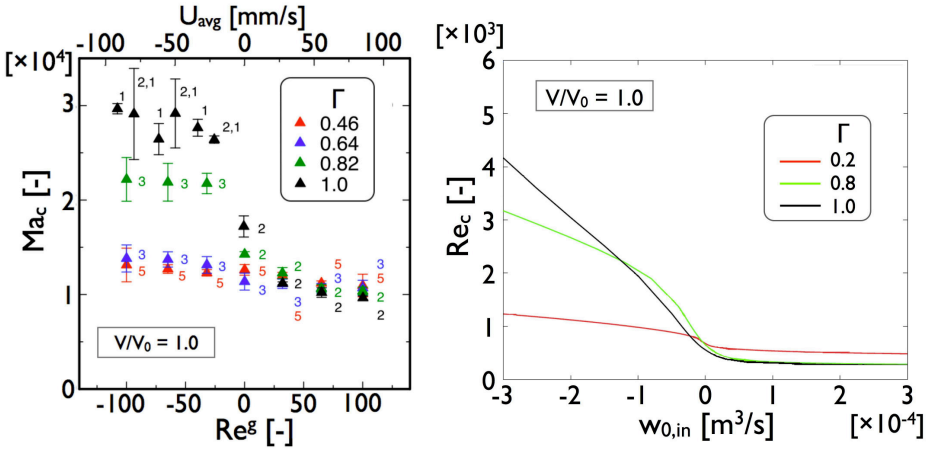

Figure 11: Effect of the ambient gas flow on the onset of oscillatory instability in a liquid bridge of various aspect ratio Γ when $V/V_0 = 1.0$; experimental results (left) for 2-cSt silicone oil ($Pr = 28.1$) are obtained by TUS, while the linear stability analysis (right) for 5-cSt silicone oil ($Pr = 67$) is due to Lukasser and Kuhlmann (private communication). The azimuthal wave mode number m is given near the symbols for the experimental results (left).

4.3.2 Stability map as function of the gas velocity and the aspect ratio

We have experimentally determined the threshold of the oscillatory instability in terms of critical Marangoni number $\mathrm{Ma_c}$ as a function of the gas-flow Reynolds number for several aspect ratios Γ. The results are shown in the left part of Fig. 11.

In all experiments of this figure the volume ratio of the liquid bridge has been kept constant at $V/V_0 = 1.0$. The azimuthal wave number m of the flow in the liquid bridge slightly above the critical point is indicated by numbers near the symbols in the plot.

The critical Marangoni number depends monotonically on the gas-flow Reynolds number, independent of Γ. This means that $\mathrm{Ma_c}$ decreases as the $\mathrm{Re^g}$ increases for $\mathrm{Re^g} > 0$, and $\mathrm{Ma_c}$ increases as the absolute value of the $\mathrm{Re^g}$ increases for $\mathrm{Re^g} < 0$. The critical Marangoni number is quite insensitive with respect to the aspect ratio and the strength of the gas flow for $\mathrm{Re^g} > 0$. For $\mathrm{Re^g} < 0$, however, $\mathrm{Ma_c}$ depends sensitively on Γ and on $\mathrm{Re^g}$. One can see that the variation of the $\mathrm{Ma_c}$ against the $\mathrm{Re^g}$ is relatively small for smaller aspect ratios (0.46 and 0.64). For larger aspect ratios (0.82 and 1.0), on the other hand, $\mathrm{Ma_c}$ increases strongly with with Γ in the case of $\mathrm{Re^g} < 0$ and even seems to exhibit a jump on a variation of $\mathrm{Re^g}$.

The results of linear stability analysis (LSA, see section4.2) shown on the right side of Fig. 11 exhibit the same qualitative dependence of the critical conditions on the ambient gas flow and on the aspect ratio Γ. The critical values determined in the experiments are given in terms of the critical Marangoni number (Ma_c), while the numerical results are presented using the thermocapillary Reynolds number $\mathrm{Re_c} = \mathrm{Ma_c}/\mathrm{Pr}$. Moreover, the ambient gas flow in the experiments is measured by the gas-flow Reynolds number (Re^g), while numerical results use the flow rate. Note, that there exist differences in the Prandtl number of the test fluid and of the ambient gas, i.e. 2-cSt silicone oil ($Pr = 28.6$) and air were used in the experiments, whereas 5-cSt silicone oil ($Pr = 67$) and argon were used for the LSA. But regardless of these differences both experiments and LSA show that a downward flow ($\mathrm{Re^g} < 0$) in the ambient gas substantially stabilizes the steady axisymmetric flow in the liquid when the aspect ratio is decreased from $\Gamma \sim 1$.

We also have been paid attention to the effect of the volume ratio of the liquid bridge V/V_0 on the critical conditions. Figure 12 illustrates the experimental results for $\mathrm{Ma_c}(V/V_0)$ for various $\mathrm{Re^g}$. The critical Marangoni number decreases almost monotonically with the volume ratio. The variation of the critical condition is most pronounced for negative values of $\mathrm{Re^g}$. The dependence of the critical Marangoni number on the volume ratio for various aspect ratios will be presented elsewhere.

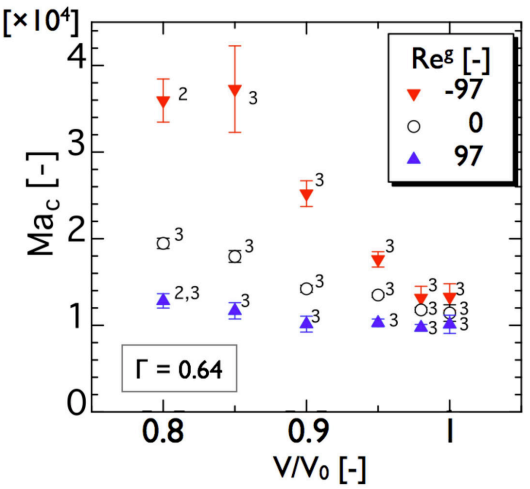

Figure 12: Critical Marangoni number as a function of V/V_0 for various $\mathrm{Re^g}$ under $\Gamma = 0.64$. Numbers near the symbols indicate the azimuthal mode number m observed in the liquid bridge above the onset of instability.

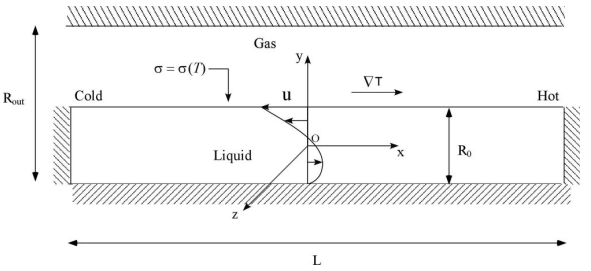

4.4 Instability mechanisms in a dynamic thermocapillary liquid layer subjected to a cold gas stream (M. Lappa)

A thorough understanding of the physics underlying the planned JEREMI experiment is of a crucial importance. Such a knowledge can provide *a priori* important insights into the dynamics to be observed in space and, accordingly, help expedite the related experimental studies. Along these lines, the work undertaken at Telespazio has been concentrated on investigating the influence of the considered thermal and kinematic boundary conditions on the *nature* of the expected flow instability. Leaving aside for a while the effective liquid bridge case, attention has been paid to the general problem related to the instability of the two-dimensional plane parallel flow which can be established in the *core* of elongated cavities (the core is the region sufficiently far away from the end regions, where the fluid turns around, to be considered not to be influenced by such edge effects, see, e.g., Lappa (2007, 2012a)). In the case of flow driven by gradients of surface tension, the related problem is generally known as the stability of the (Marangoni) return flow. In spite of considerable research and efforts deployed by different research groups, such a fundamental case does not seem to have received the deserved attention. Even though limited to cases of great simplicity (excluded are any processes that depend on curvature of the liquid/gas interface or the inherent property of the system of being cylindrical), these two-dimensional solutions have proved able to yield directly or indirectly insights and understanding that would have been difficult to obtain otherwise. In the simplified situation of adiabatic free interface and no gas flow (classical problem already considered in the literature, see, e.g., Lappa (2005, 2010) and references therein), it is known that the basic-state temperature field contains a flow-induced vertical temperature distribution corresponding to a layer being cooled from below. For this case, the socalled *hydrothermal waves* always correspond to the preferred mode of instability. This oscillatory mechanism was investigated theoretically by Smith and Davis (1983) (indeed, they were the first to coin the related denomination hydrothermal waves). These waves are known to be almost two–dimensional in the high-Pr case (Peltier and Biringen (1993); Xu and

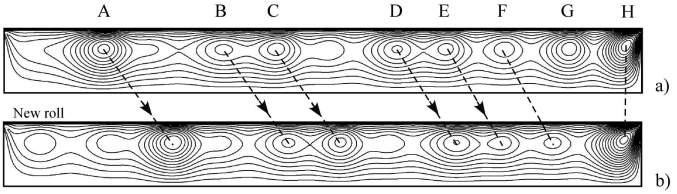

Figure 13: Oscillatory instability of Marangoni flow in a liquid layer with adiabatic interface (Pr=68, Γ=20, $Ma_{layer} = 7 \times 10^4$, $Re_g = 0$; cold side on the left, hot side on the right; the isolines of the stream-function are shown in two snapshots during one period of oscillation): The location of the cells at different time moments indicates a propagation to the right, i.e. in the upstream direction (for illustration purposes, in the figure above the depth of the fluid layer is two times its real dimension; all rolls rotate in the anti-clockwise sense; the non-dimensional angular frequency of the wave is $\omega \approx 64.74$, ω being referred to the time scale R_0^2/ν^l)

Zebib (1998); Tang and Hu (2005)). A remarkable feature common to all cases is that the disturbance always travels in a direction with a component in the direction opposite to that of the surface flow (upstream).

Another interesting feature of this kind of flow is the absence of stationary convective instabilities. Like the Pearson's instability (Pearson (1958)), the presence of temperature disturbances on the free surface, however, is an essential ingredient of the hydrothermal mechanism. It is known, in fact, that this kind of instability cannot occur when the free surface behaves as a perfectly conducting boundary (see Lappa (2010) for the necessary mathematical background). Conversely, mechanisms as those described, e.g., by Smith (1986) can be retained if the free surface is allowed to exchange heat with the ambient (Priede and Gerbeth, 2003).

Although our geometry is not cylindrical, for consistency we use the nomenclature defined in Sect. 3 and refer the reader to that section for the necessary background in terms of symbols, relevant equations and characteristic numbers. In particular, the following conditions are considered: Pr=68 (5cSt silicone oil), H_c=0, H_h=0, Γ=20, Gr=0, $Ma = Ma_{layer}\Gamma$, $Ma_{layer} = 7 \times 10^4$ (based on the layer depth), Γ_R=2, $\tilde{\mu} = 255$, $\tilde{k}$ =5.1, $\tilde{\nu}$=0.29, Re_g=300 (gas injected from the cold side), where Re_g is defined as $(R_{out} - R_0)U_0^g/\nu^g$.

For no gas flow and adiabatic interface, a strong cell structure is formed in the region close to the hot wall (labeled as H in Fig. 13, such a stationary roll existing near the right wall is basically maintained by the strong temperature gradient established in the lateral boundary layer), while the hydrothermal wave is manifested by the propagation of well-defined convective structures from the cold side towards the hot one, (Smith and Davis, 1983). As shown in Fig. 13, the hydrothermal

wave looks as a succession of cells moving from the cold side towards the motionless rolls on the hot side. This wave "feels" the presence of the steady roll H by decaying in the region where this roll is located; when a roll *dies* (see, e.g., the roll labeled G), a new roll is created at the cold side thereby preserving the overall number of rolls present in the cavity at any instant.

The numerical simulations, however, show that if gas (air) is injected from the cold side (at the same initial temperature of the cold sidewall and with a uniform velocity profile along the vertical coordinate y), the scenario can change dramatically. For Re_g=300 (Fig. 14) the exchange of momentum between the gas and the liquid layer is such that regions of reversed flow direction are created at the free/liquid gas interface.

In particular, at any moment the flow pattern can be split ideally in four independent circulation systems:
A quasi-steady (motionless) roll, driven by the strong temperature gradient established in the lateral boundary layer, stays attached to the hot wall (as in the case with no gas seen in Fig. 13). A group of cells spatially spreading periodically towards the cold side (i.e. *moving downstream*), represents a second independent circulation system. Such a group of rolls is bounded from the right (where such rolls are being continuously created) by the above mentioned strong convective cell and from the left (where they decay) by a third region where convection displays again a quasi-steady behavior. This region is characterized by a relatively stable pattern consisting of two distinct couples of counter-rotating rolls. Although the two couples of rolls undergo a limited weak (back and forth) motion along the horizontal direction, they occupy relatively stable positions (thereby, creating a 'barrier', i.e. a resistance to the propagation of the rolls being continuously created at the hot side and spreading towards the cold side along the second region). As anticipated, under the impact of the moving rolls coming from the hot side, all the rolls that belong to the multicellular structure in region 3 oscillate weakly in time (the amplitude of the velocity oscillations at a fixed point in region 3 is many times smaller than that at a fixed point located in region 2). Finally, a fourth independent region can be identified in proximity to the cold wall, where the local patterning behavior consists of the alternation of two distinct co-rotating rolls and a single vortex formed by the periodic merging of such rolls.

Comparison of Fig. 14 with Fig. 13 indicates that, since for the case of no gas flow and adiabatic interface the wave spreads from the cold to the hot side, whereas, when gas injected form the cold side is considered, a region exists where the oscillations propagate in the opposite direction, these disturbances may be of a different nature (such a conclusion being also supported by the fact that the oscillation frequency of the multicellular flow in region 2 is many times higher than the frequency

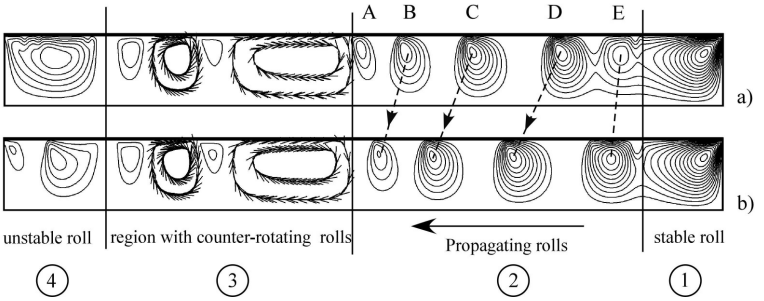

Figure 14: Oscillatory instability of Marangoni flow in a liquid layer with gas stream from the cold side (Pr=68, Γ=20, $Ma_{layer} = 7 \times 10^4$, Re^g=300; cold side on the left, hot side on the right; the isolines of the stream-function are shown in two snapshots; all solid-line arrow-less rolls rotate in the anticlockwise sense, rotation in the clockwise sense is expressly highlighted by the use of arrows). A region exists where the evolution of the cells at different time moments indicates a propagation to the left, i.e. in the downstream direction (the related nondimensional angular frequency is $\omega \approx 1 \times 10^3$, ω being referred to the time scale R_0^2/ν^l)

of the HTW seen in Fig. 13).

The most interesting insights into these phenomena, however, are obtained when the temperature distribution is examined (Figs. 15 and 16). When the interface is adiabatic, the temperature profile is such that a generic point at the free surface is hotter than other points located (at the same coordinate) below the interface (i.e. a positive vertical temperature gradient exists, Fig. 15). When the cold gas flow is considered, however, for the present conditions (Re^g=300), it can be clearly seen that the region affected by the rolls propagating towards the cold side displays a temperature profile where the situation described above is reversed (in terms of temperature variation along the vertical direction in proximity to the interface, the vertical temperature gradient is negative, Fig. 16).

Such observations, if properly interpreted in the light of the arguments developed earlier on the nature of the instability, lead to the general conclusion that in the presence of a cold gas current entering the system from the left (cold) side, the classical hydrothermal wave (typical of high–Pr liquids where disturbances derive their energy from the vertical temperature gradient through vertical convection, Smith (1986)) may be taken over by a different mechanism. Although disturbances will still derive their energy from the vertical temperature gradient through vertical convection, however (given the reversed sign of the vertical temperature gradient), effects similar to those typical of the Pearson (Marangoni–Bénard) instability should be expected.

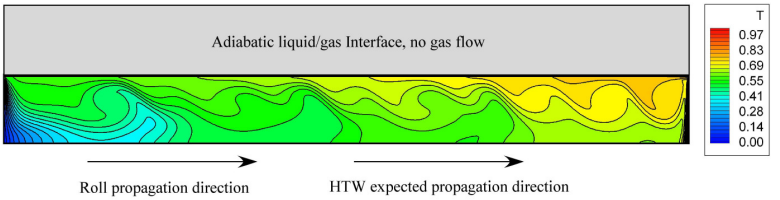

Figure 15: Snapshot of temperature distribution for the same conditions considered in Fig. 13

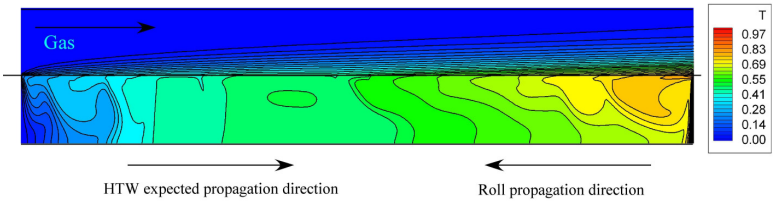

Figure 16: Snapshot of temperature distribution for the same conditions considered in Fig. 14

Albeit, technically speaking, the Pearson (Marangoni-Bénard) instability is a stationary bifurcation, we ascribe the observed motion of the rolls (towards the cold side) to the fact that, unlike the classical Marangoni-Bénard problem, in the present case the unstructured (initial) base state in the cavity is characterized not only by a vertical temperature gradient but also by a symmetry-breaking shear flow (the Marangoni surface stresses driven by the imposed horizontal temperature gradient imply vertical gradients of horizontal velocity). By breaking the in-plane isotropy of the usual horizontal layer heated from below, the presence of this shear flow may explain the observed departure of the dynamics from well-known Marangoni-Bénard (stationary) dynamics.

In general, these results support the recent findings by Shevtsova, Gaponenko, and Nepomnyashchy (2013), who found similar behaviors and came to similar conclusions in the liquid bridge case.

4.5 Dynamic interface deformations due to thermocapillary and shear stresses

4.5.1 Numerical study of dynamic interface deformations due to shear stresses (J. M. Montanero)

In this section, we analyze the mechanical behavior of an isothermal liquid bridge immersed in a coaxial gas stream, paying particular attention to the liquid velocity field and the free surface deformation caused by the gas stream. For this purpose,

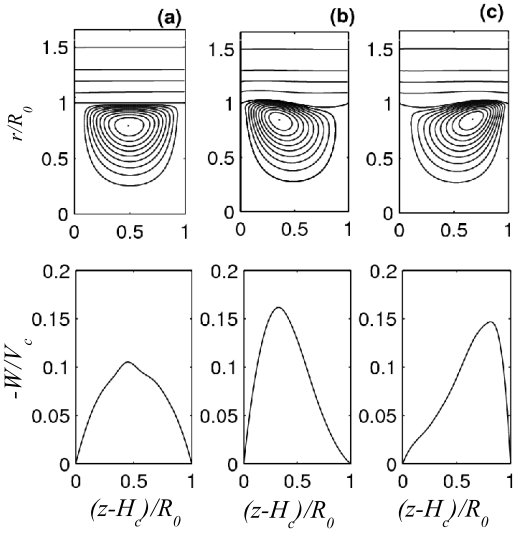

Figure 17: Streamlines (upper graphs) and axial component of the velocity at the free surface (lower graphs) for $|w^g|_{max}/V_c = 28.11$ and $Bo = 0$ (a), $Bo = 4.06$ (b), and $Bo = -4.06$ (c).

the full Navier-Stokes equations were solved numerically with GERRIS, an Open Source Free Software library developed by Popinet (2003, 2009). We considered the boundary conditions mentioned in Sec.3.2, except at both the inlet and the outlet of the gas, where the fully developed flow condition for an annulus was prescribed (Herrada, López-Herrera, Vega, and Montanero, 2011).

The geometrical parameters were: $R_0 = 3$ mm, $R_{out} = 5$ mm, and $d = 3$ mm. The liquid bridge volume was that of the cylinder delimited by the two rods. The working liquid was 5-cSt silicone oil ($\rho^l = 919$ kg/m^3, $\mu^l = 4.60 \times 10^{-3}$ kg/ms, and $\sigma = 0.020$ N/m), while the gas was air at normal conditions ($\rho^g = 1.22$ kg/m^3 and $\mu^g = 1.7 \times 10^{-5}$ kg/ms). This parameter set was also considered by Gaponenko, Ryzhkov, and Shevtsova (2010). The corresponding dimensionless parameters characterizing the fluid configuration were: $\Gamma = 1$, $\Gamma_R = 1.67$, $\mathscr{V} = 1$, $\widetilde{\mu} = 271$, $Ca = 3.84 \times 10^{-4}$, and $Bo = 0$ (zero gravity) or $Bo = \pm 4.06$ (normal gravity conditions), where the positive (negative) sign applies when the gas flow and gravity force have the same (opposite) directions. We considered several values of the gas-flow rate, as indicated by the maximum magnitude of the axial velocity component at the gas inlet, $|w^g|_{max}$. In the set of dimensionless numbers, the gas Reynolds number Re_g was replaced by $|w^g|_{max}$ measured in terms of the capillary velocity $V_c = R_0/t_c$, where t_c is the capillary time $t_c = (\rho^l R_0^3/\sigma)^{1/2}$.

The simulation started from a cylindrical liquid bridge at rest immersed in a coaxial

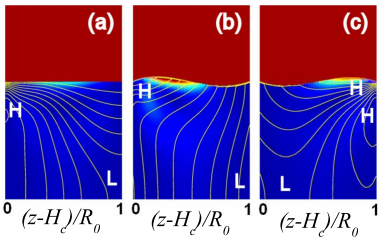

Figure 18: (Color online) Reduced pressure and kinetic energy distributions for $|w^g|_{max}/V_c = 56.34$ and $Bo = 0$ (a), $Bo = 4.06$ (b), and $Bo = -4.06$ (c). The lines in the liquid bridge are isobars. The high and low pressure regions are indicated by the labels H and L, respectively. The colors blue and red correspond to the lowest and highest kinetic energy values, respectively.

gas stream with a velocity field corresponding to the fully developed flow condition in the entire gas domain (Herrada, López-Herrera, Vega, and Montanero, 2011). For $Bo \neq 0$, moderately large free surface oscillations appeared in the transient regime due to gravity. Figures 17-20 show the results obtained in the steady regime. The streamlines in both the liquid and gas domains for zero (a) and normal (b and c) gravity conditions are plotted in the upper graphs of Fig. 17. A recirculation cell is set in motion driven by the viscous shear stress exerted over the interface by the gas stream flowing leftwards. The liquid moves leftwards in a boundary layer close to the free surface. In the left part of the liquid bridges (a) and (b), momentum accumulates (see Fig. 18), the reduced pressure increases, and the liquid is pumped rightwards through the bulk. On the contrary, liquid inertia has to overcome the adverse reduced pressure gradient in the bulk for $Bo < 0$. As shown in the lower graphs of Fig. 17, the velocity distribution over the free surface considerably depends on the Bond number value.

The mechanism driving the liquid recirculation for $Bo \geq 0$ is more energetically efficient than that of the case $Bo < 0$. In the former case, viscous tangential stress exerted by the gas stream and the favorable reduced pressure force collaborate with each other to keep the liquid in motion: while the formed makes the liquid move downwards in the boundary layer, the latter helps the liquid flow back through the bulk. On the contrary, both viscous tangential stresses and pressure forces push the liquid in the same direction through the boundary layer for $Bo < 0$. The kinetic energy accumulated in this first stage of the motion is used to overcome the adverse reduced pressure gradient in the liquid bridge bulk. This results in a greater kinetic energy dissipation which reduces significantly the recirculation speed. The values of both the vorticity and the viscous dissipation function are consistent with the above explanation (Herrada, López-Herrera, Vega, and Montanero, 2011).

Both the maximum value w^l_{max} of the axial velocity component in the liquid domain, and the recirculating flow rate $Q_r = \pi \int_0^{h(z)} |w(r,z)|\ r\ dr$, are plotted in Fig. 19 for $(z-H_c)/R_0 = 0.5$. The dependency with respect to the gas speed is quasi-linear for the range of velocities considered. We verified that the liquid bridge breaks

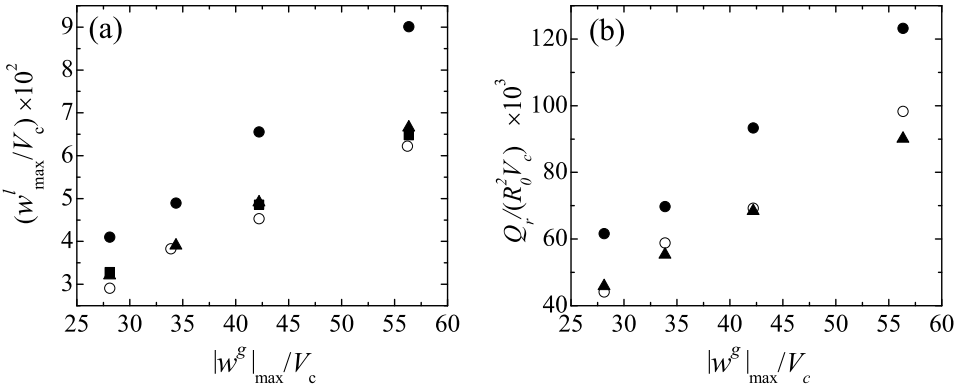

Figure 19: Maximum value w^l_{max} of the axial velocity component measured in the liquid (a) and recirculating flow rate Q_r (b) as a function of $|w^g|_{max}$ for $Bo = 0$ (open symbols), $Bo = 4.06$ (circles), and $Bo = -4.06$ (triangles). The squares in (a) correspond to the simulations for $Bo = 0$ with a rigid free surface.

up for $|w^g|_{max}/V_c \sim 60$. For $Bo > 0$, the liquid bridge moves much faster than in the other two cases, which can be explained as follows. Gravity turns a cylindrical free surface into an amphora-type shape. The gas accelerates close to the free surface delimiting the bulging region of the liquid bridge due to simple continuity arguments, which increases the viscous stress there. The momentum transferred to the liquid in that region also increases, which results in a faster recirculation cell. The same argument could be also applied to the case $Bo < 0$. However and as explained above, the recirculation cell in this case is more dissipative than for $Bo \geq 0$, which hinders significantly its motion.

Figure 19a also shows the results calculated when the interface is regarded as a rigid cylindrical boundary. In this case, the velocity component normal to the interface vanishes, while the tangential velocity component and the stresses take the same values on both sides of the free surface. While these simplifications accelerate significantly the calculations, they still lead to relatively accurate predictions for w^l_{max}.

Figure 20a shows the interface deformation $h - h_0$ with respect to the equilibrium shape h_0 for different gas velocities. For $Bo \geq 0$, the recirculation pattern made the

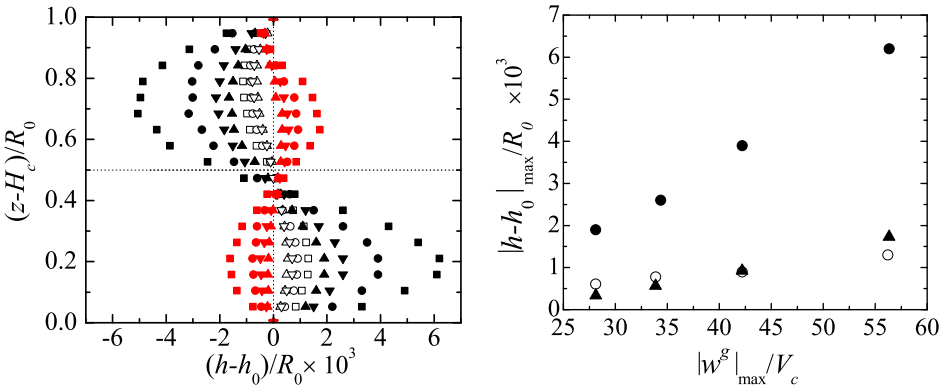

Figure 20: (Left, Color online) Interface deformation $h - h_0$ for $Bo = 0$ (open symbols), $Bo = 4.06$ (black symbols), and $Bo = -4.06$ (red symbols). The up-triangles, down-triangles, circles, and squares correspond to $|w^g|_{max}/V_c = 28.11$, 34.37, 42.20, and 56.34, respectively. (Right) Maximum magnitude $|h - h_0|_{max}$ of the interface deformation as a function of $|w^g|_{max}$ for $Bo = 0$ (open symbols), $Bo = 4.06$ (circles), and $Bo = -4.06$ (triangles).

hydrostatic pressure increase in the lower part of the liquid bridge, which bulged in that region. The interface deformation for $Bo = 4.06$ was significantly larger than in the absence of gravity for two reasons. Firstly, the liquid bridge was closer to its stability limit for $Bo = 4.06$ (Slobozhanin and Perales, 1993), and thus its shape was more sensitive to variations in the pressure distribution; and (ii) as mentioned above, the liquid bridge moved much faster for $Bo = 4.06$ than in the absence of gravity, and thus the increase of hydrostatic pressure in the lower region was considerably higher for the former case. Interestingly, the shape and magnitude of that deformation resembles that produced by thermal convection in high-Prandtl-number liquid bridges (Montanero, Ferrera, and Shevtsova, 2008). For $Bo = -4.06$, the deformation shape is the opposite because the hydrostatic pressure decreases (increases) in the lower (upper) part of the liquid bridge. The deformation magnitude is similar to that of the case $Bo = 0$, as occurs with the recirculation speed. The static (due to gravity) and dynamic deformations have the same shape for both $Bo > 0$ and $Bo < 0$. Therefore, one may expect that the gravitational force collaborates with the gas stream in destabilizing the liquid bridge.

The maximum magnitude $|h - h_0|_{max}$ of the free surface deformation is shown in Fig. 20b as a function of the gas velocity. A linear dependency is observed for both weightless and normal gravity conditions. In all the cases, the deformation caused by the gas stream was less than 20 μm, much smaller than that associated with gravity (for instance, the maximum static deformation $|h_0 - 1|_{max}$ is about 100 μm

for the liquid bridge considered in this section). One does not expect the dynamical interface deformation to alter considerably the liquid bridge response to thermal gradients.

4.5.2 *Measurements of the dynamic surface deformation due to shear stresses (A. Mialdun, K. Nishino, V. Shevtsova)*

The dynamic free-surface deformations induced by flow are experimentally studied in a confined liquid volume of 5cSt silicone oil (Prandtl number $Pr = 68$). The geometry of the problem is a vertical liquid column concentrically surrounded by an annular gas channel. A gas stream entering the duct from the top or bottom carries the motionless liquid. The dynamic deformation of the gas–liquid interface is caused by a steady axisymmetric shear-driven flow. The experiments are performed in normal gravity conditions and the static deformation of a liquid bridge interface is unavoidable.

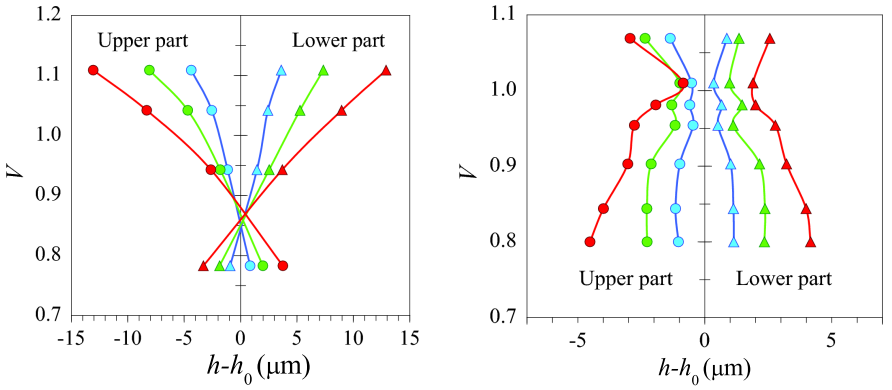

Figure 21: Extrema of the dynamic deformation at upper (circles) and lower (triangles) parts of a liquid bridge as a function of volume ratio $\mathscr{V}$. The different curves with symbols (in order by the distance from the axis) correspond to the gas velocity U_0^g= 1m/s, 1.5m/s and 2 m/s. (left) Gas enters from the bottom. (right) Gas enters from the top.

The magnitude and shape of the dynamic surface deformation were analyzed using optical measurements with a comprehensive treatment of the images. The deviation of the free surface shape from the corresponding equilibrium profile is determined with an uncertainty of about $0.1\mu m$. The order of magnitude of the interface deformation is proportional to the capillary number, which is defined as the ratio of the viscous force per unit area to the capillary pressure. The study is performed for a large range of volumes and aspect ratios as well as for different gas velocities Matsunaga, Mialdun, Nishino, and Shevtsova (2012).

As a general trend, the dynamic deformation grows with the gas velocity, which plays the role of a driving force, but a linear dependence is not observed for all volume ratios, despite the small Reynolds numbers, $280 < Re_g < 560$. The dynamic deformation displays a strong dependence on the liquid volume ratio and the direction of the gas stream parallel to the interface. When the gas flow is directed against gravity, the largest interface deformations are observed at the smallest volumes among the analyzed ones, see Fig.21 (right). In contrast, when the gas stream

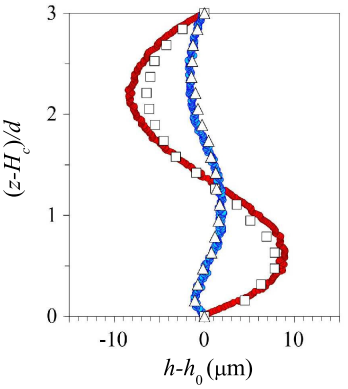

Figure 22: Interface deformation by flow $(h - h_0)$ when $\mathscr{V} = 1$, $\Gamma = 1$, and $U_0^g = 2\,m/s$. Comparison of the experimental (closed symbols) and numerical (open symbols) results when gas enters from the top (squares) and bottom (triangles). The numerical results are taken from the paper by Herrada, López-Herrera, Vega, and Montanero (2011).

is aligned with gravity, then the deformations decrease with a decrease in the volume ratio, at a certain value attaining zero (vanishing) and then changing sign, see Fig.21 (left).

The dynamic deformation for the volume ratio $\mathscr{V} = 1$ has been recently calculated by Herrada, López-Herrera, Vega, and Montanero (2011) for both directions of gas when U_0^g = 2 m/s. A comparison of the results is shown in Fig.22, where the closed symbols correspond to the experiments in this work and the open symbols correspond to the numerical results. An excellent agreement is observed in the case when gas enters from the bottom. For the direction of gas from top to bottom, the agreement is less perfect but still satisfactory. These comparisons with the numerical results (Herrada, López-Herrera, Vega, and Montanero (2011), Gaponenko, Glockner, Mialdun, and Shevtsova (2011)) show that the experimental technique is able to give smooth and feasible results in a broad range of volume ratios and shear stresses.

4.5.3 Measurements of the dynamic surface deformation caused by a thermocapillary flow (J.M. Montanero, V. Shevtsova)

This section closes with some experimental results on the free surface deformation when a temperature difference ΔT is applied between the liquid bridge supporting rods. The dynamical free surface deformation induced by buoyancy and thermocapillary convection in non-cylindrical liquid bridges of 5-cSt silicone oil was measured in both the steady and oscillatory regimes. The supercritical free surface shape is the superposition of the static shape, the steady dynamical deformation due to the basic flow, and the small-amplitude free surface oscillations caused by the oscillatory instability.

The steady dynamic deformations of the interface were studied in two experimental runs. The radius of the rods was $R_0 \simeq 3$ mm, while the distance between them was $d \simeq 3.6$ mm. Two dimensionless volumes were considered: $\mathscr{V} = 0.8200$ [experimental run (I)] and $\mathscr{V} = 0.8764$ [experimental run (II)]. The ranges of applied temperature difference were $0 \leq \Delta T \leq 32$ K and $0 \leq \Delta T \leq 38$ K for the runs (I) and (II), respectively. The analysis of the temperature series measured by the thermocouples revealed that the oscillatory instability appeared at ΔT = 16.80 and 16.55 K for the runs (I) and (II), respectively (Montanero, Ferrera, and Shevtsova (2008)).

For each ΔT, ten images were acquired to measure the average value $\langle h \rangle - h_0$. If the temperature difference is smaller than the critical value, then this quantity is the free surface deformation caused by the steady axisymmetric thermal convection. On the contrary, for supercritical values of ΔT, $\langle h \rangle - h_0$ is a good approximation to

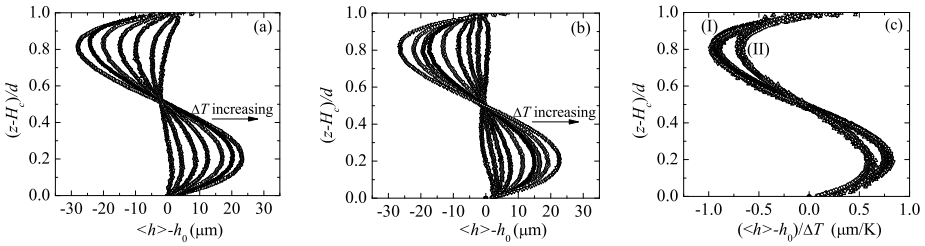

Figure 23: Dynamic free surface deformation $\langle h \rangle - h_0$ at different ΔT for the experimental runs (I) (a) and (II) (b). The values of the applied temperature difference were ΔT = 1.04, 5.46, 11.05, 15.20, 21.76, 25.33, and 31.26 K [run (I)], and ΔT = 0.01, 3.90, 7.46, 12.03, 18.18, 24.39, 28.39, 32.70, and 37.20 K [run (II)]. The plots (c) shows the dynamic free surface deformations presented in plots (a) and (b) normalized by ΔT.

the average of the free surface deformation over the oscillation period, and hence

can be seen as the deformation caused by the axisymmetric steady flow that underlies that oscillation. The free surface deformation shown in Figs. 24 *a* and 24 *b* monotonically increased with ΔT in the two experimental runs. The remarkable result of the experimental study is that the deviation of the free surface shape from the static one grew linearly with ΔT both below and above the onset of instability, Fig. 23 *c*, and its maximum value over the free surface had the same order of magnitude as that of the Capillary number ($Ca = \Gamma \Delta T / \sigma_0$). This tendency was also confirmed numerically (see Shevtsova, Mialdun, Ferrera, Ermakov, Cabezas, and Montanero (2008)).

The experiment did not reveal any significant difference between the results obtained in the steady axisymmetric and oscillatory regimes for the mean deformation. In other words, the hydrothermal waves that appeared in the oscillatory regime as ΔT increased did not significantly modify the behavior of the mean deformation shape. The amplitude of the interface oscillations was accurately measured in

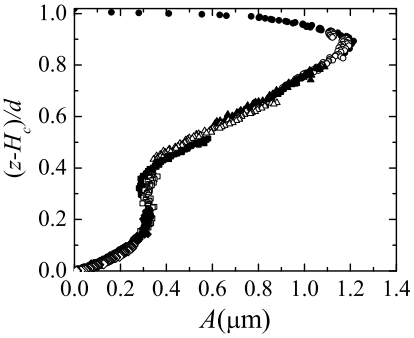

Figure 24: ((b) Measured z-dependence of oscillations amplitude over the whole height of the liquid bridge, 5 cSt silicone oil, $\mathscr{V}$ =0.88 and ΔT =25.8°C while ΔT_{cr} =16.6°C. Various symbols correspond to the results from the different displacements of the CCD camera.

a liquid bridge with volume $\mathscr{V} = 0.88$ when $\Delta T \approx 1.6 \Delta T_{cr}$ (Ferrera, Montanero, Mialdun, Cabezas, and Shevtsova (2008)). Figure 24 demonstrates a strong z-dependence of the oscillations amplitude. The greatest change in amplitude occurs at the upper part, but even in this region, the deformation is one order of magnitude smaller than the average dynamic deformation. However, despite smallness of the amplitude, the appearance of the sustained interface oscillations enables the measurements of the threshold of the oscillatory instability.

5 Conclusions

The geometry of the physical problem under consideration is a cylindrical liquid bridge concentrically surrounded by an annular gas channel. The gas flow in the annular channel provides two actions on the motion in the liquid: via shear stresses and via cooling/heating the gas–liquid interface. The role of shear stresses diminishes with an increase of the liquid–gas-viscosity ratio. In future microgravity experiments this ratio will be large, $\mu^l/\mu^f = 217$, (5cSt silicone oil/Argon) and the thermal effect will play a dominant role. The problem is multi-parametric and requires experiments and calculations in a wide parameter space. The target of the preparatory studies presented is to identify the most important control parameters. We have developed a few three-dimensional numerical codes for one- and two-phase simulations and different experimental setups.

Two-phase simulations allow to determine the Biot number as a function of the gas-flow rate, which can then be used in a single-phase model. The performed simulations as well as the experiments show that for moderate values of the Reynolds number, $|Re^g| \leq 100$, the Biot number increases monotonically when Re^g grows and changes sign from negative to positive. In the case of a passive gas the Biot number is in the range $0.2 - 0.5$.

The stability diagram of the flow as a function of the gas-flow rate displays a non-unique behaviour depending on the velocity and temperature of gas. Generally, a more intriguing behaviour occurs when gas enters from the cold side (the net gas flow opposes the surface flow) where 2D, 3D oscillatory and 3D stationary instabilities are observed at relatively low Marangoni numbers.

The numerical and experimental analysis for 5cSt silicone oil shows that the surface deformation due to the gas flow for the above range of Reynolds numbers is not significant, about $1 - 10\mu m$ depending on the flow direction and the gravity level. Approximately the same magnitude of the surface deformation, $10 - 20\mu m$, is caused by the thermocapillary flow itself in the absence of a forced gas flow. For theses reasons dynamic free-surface deformation can be neglected in numerical models if the Reynolds number in the gas phase satisfies $|Re^g| \leq 100$.

Acknowledgments

The authors of Section 4.1 gratefully acknowledge the PRODEX programme of the Belgian Federal Science Policy Office and ESA.

The authors of Section 4.2 gratefully acknowledge support from ESA (contract number 4000103003) and BMVIT (ASAP-6 contract number 819714.

The authors of Section 4.3 gratefully acknowledg financial support of 'Grant-in-

Aid for Scientific Research (B) (Research Project Number: 24360078)' by the Japan Society for the Promotion of Science (JSPS) for the research activities on this topic at the Tokyo University of Science. The data indicated here had been accumulated by Mr. Akira Kawazoe and Mr. Yusuke Makino, the former graduate students of Tokyo University of Science.

The author of Section 4.4 acknowledges support from ASI (contract I/048/11/0).

References

Chun, C.-H.; Schwabe, D. (1982): Marangoni convection in floating zone. In Zierep, J.; Oertel, H.(Eds): *Convective transport and instability phenomena*, pp. 297–317. Braun, Karlsruhe.

Dressler, V. R.; Sivakumaran, N. (1988): Non-contaminating method to reduce marangoni convection in microgravity float zones. *J. Crystal Growth*, vol. 7, pp. 148–158.

Ferrera, C.; Montanero, J.; Mialdun, A.; Cabezas, M.; Shevtsova, V. (2008): A new experimental technique for measuring the dynamical free surface deformation in liquid bridges due to thermal convection. *Meas Sci Technol*, vol. 19, pp. 1–10.

Frank, S.; Schwabe, D. (1997): Temporal and spatial elements of thermocapillary convection in floating zones. *Experiments in Fluids*, vol. 23, pp. 234 – 251.

Gaponenko, Y.; Glockner, S.; Mialdun, A.; Shevtsova, V. (2011): Study of a liquid bridge subjected to interface shear stresses. *Acta Astronautica*, vol. 69, pp. 119–126.

Gaponenko, Y.; Mialdun, A.; Shevtsova, V. (2012): Shear driven two-phase flows in vertical cylindrical duct. *Int. J. Multiphase Flow*, vol. 39, pp. 205 – 215.

Gaponenko, Y.; Ryzhkov, I.; Shevtsova, V. (2010): On flows driven by mechanical stresses in a two-phase system. *Fluid Dyn. Mat. Proc.*, vol. 6, pp. 75 – 97.

Gaponenko, Y.; Shevtsova, V. (2012): Heat transfer through the interface and flow regimes in liquid bridge subjected to co-axial gas flow. *Microgravity Sci. Technol.*, vol. 24, pp. 297 – 306.

Herrada, M. A.; López-Herrera, J. M.; Vega, E. J.; Montanero, J. M. (2011): Numerical simulation of a liquid bridge in a coaxial gas flow. *Phys. Fluids*, vol. 23, pp. 012101.

Irikura, M.; Arakawa, Y.; Ueno, I.; Kawamura, H. (2005): Effect of ambient fluid flow upon onset of oscillatory thermocapillary convection in half-zone liquid bridge. *Microgravity Sci. Technol.*, vol. 16, pp. 174 – 180.

Kamotani, Y.; Wang, L.; Hatta, L.; Wang, A.; Yoda, S. (2003): Free surface heat loss effect on oscillatory thermocapillary flow in liquid bridges of high prandtl number fluid. *Intl J. Heat Mass Transfer*, vol. 46, pp. 3211 – 3220.

Kawamura, H.; Nishino, K.; Matsumoto, S.; Ueno, I. (2010): Space experiment of Marangoni convection on International Space Station. In *Proceedings of the 14th International Heat Transfer Conference*. ASME.

Kousaka, Y.; Kawamura, H. (2006): numerical study on the effect of heat loss upon the critical marangoni number in a half-zone liquid bridge. *Microgravity Sci. Technol.*, vol. 18, pp. 141 –145.

Kuhlmann, H.; Lappa, M.; Melnikov, D.; Mukin, R.; Muldoon, F.; Pushkin, D.; Shevtsova, V.; Ueno, I. (2014): The JEREMI-Project on thermocapillary convection in liquid bridges. Part A: Overview of particle accumulation structures. *Fluid Dyn. Mat. Proc.*, vol. 10, pp. 1–36.

Kuhlmann, H. C. (1999): *Thermocapillary Convection in Models of Crystal Growth*, volume 152 of *Springer Tracts in Modern Physics*. Springer, Berlin, Heidelberg.

Kuhlmann, H. C.; Wanschura, M.; Rath, H. J.; Yoda, S. (2000): Stability of thermocapillary flows in high-Prandtl-number liquid bridges. *Space Forum*, vol. 6, pp. 25–30.

Lappa, M. (2005): Thermal convection and related instabilities in models of crystal growth from the melt on earth and in microgravity: Past history and current status. *Cryst. Res. Technol.*, vol. 40, pp. 531–549.

Lappa, M. (2007): Secondary and oscillatory gravitational instabilities in canonical three-dimensional models of crystal growth from the melt, part2: Lateral heating and the hadley circulation. *Comptes Rendus Mécanique*, vol. 335, pp. 261–268.

Lappa, M. (2010): *Thermal Convection: Pattern, Evolution and Stability*. John Wiley & Sons, Chichester, United Kingdom.

Lappa, M. (2012a): Exact solutions for thermal problems: Buoyancy, marangoni, vibrational and magnetic-field-controlled flows. *Review of Applied Physics*, vol. 1, pp. 1–14.

Lappa, M. (2012b): *Rotating Thermal Flows in Natural and Industrial Processes*. John Wiley & Sons, Chichester, United Kingdom.

Levenstam, M.; Amberg, G.; Winkler, C. (2001): Instabilities of thermocapillary convection in a half-zone at intermediate Prandtl numbers. *Phys. Fluids*, vol. 13, pp. 807–816.

Leypoldt, J.; Kuhlmann, H. C.; Rath, H. J. (2000): Three-dimensional numerical simulation of thermocapillary flows in cylindrical liquid bridges. *J. Fluid Mech.*, vol. 414, pp. 285–314.

Lowry, B.; Steen, P. (1997): Stability of slender liquid bridges subjected to axial flows. *J. Fluid Mech.*, vol. 330, pp. 189–213.

Matsunaga, T.; Mialdun, A.; Nishino, K.; Shevtsova, V. (2012): Measurements of gas/oil free surface deformation caused by parallel gas flow. *Phys. Fluids*, vol. 24, pp. 062101.1 – 062101.17.

Melnikov, D.; Shevtsova, V.; Legros, J. (2004): Onset of temporal aperiodicity in high prandtl number liquid bridge under terrestrial conditions. *Phys. Fluids*, vol. 16, pp. 1746 – 1757.

Mialdun, A.; Shevtsova, V. (2006): Influence of interfacial heat exchange on the flow organization in liquid bridge. *Microgravity Sci. Technol.*, vol. 18, pp. 146 – 149.

Montanero, J.; Ferrera, C.; Shevtsova, V. (2008): Experimental study of the free surface deformation due to thermal convection in liquid bridges. *Experiments in Fluids*, vol. 45, pp. 1087 – 1101.

Nepomnyashchy, A.; Simanovskii, I.; Braverman, L. (2001): Stability of thermocapillary flows with inclined temperature gradient. *J. Fluid Mech.*, vol. 442, pp. 141–155.

Pearson, J. (1958): On convection cells induced by surface tension. *J.Fluid Mech.*, vol. 4, pp. 489–500.

Peltier, L.; Biringen, S. (1993): Time-dependent thermocapillary convection in a rectangular cavity: numerical results for a moderate prandtl number fluid. *J.Fluid Mech.*, vol. 257, pp. 339–357.

Popinet, S. (2003): Gerris: a tree-based adaptive solver for the incompressible Euler equations in complex geometries. *J. Comput. Phys.*, vol. 190, pp. 572–600.

Popinet, S. (2009): An accurate adaptive solver for surface-tension-driven interfacial flows. *J. Comput. Phys.*, vol. 228, pp. 5838–5866.

Priede, J.; Gerbeth, G. (2003): Influence of thermal boundary conditions on the stability of thermocapillary-driven convection at low prandtl numbers. *Phys. Fluids*, vol. 9, pp. 1621–1634.

Ryzhkov, I.; Shevtsova, V. (2012): Thermocapillary instabilities in liquid columns under co- and counter-current gas. *Intl J. Heat Mass Transfer*, vol. 55, pp. 1236 – 1245.

Schwabe, D. (2014): Thermocapillary liquid bridges and marangoni convection under microgravity results and lessons learned. *Microgravity Sci. Technol.*, pp. 1–10.

Schwabe, D.; Preisser, F.; Scharmann, A. (1982): Verification of the oscillatory state of thermocapillary convection in a floating zone under low gravity. *Acta Astronautica*, vol. 9, pp. 265–273.

Shevtsova, V.; D., D. M.; Legros, J. (2003): Multistability of the oscillatory thermocapillary convection in liquid bridge. *Phys. Rev.* E, vol. 68, pp. 066311.1 – 066311.13.

Shevtsova, V.; Gaponenko, Y.; Nepomnyashchy, A. (2013): Thermocapillary flow regimes and instability caused by a gas stream along the interface. *J. Fluid Mech.*, vol. 714, pp. 644 – 670.

Shevtsova, V.; Mialdun, A.; Ferrera, C.; Ermakov, M.; Cabezas, M.; Montanero, J. (2008): Subcritical and oscillatory dynamic surface deformations in non-cylindrical liquid bridges. *Fluid Dyn. Mat. Proc.*, vol. 4, pp. 43–54.

Shevtsova, V.; Mialdun, A.; Mojahed, M. (2005): A study of heat transfer from liquid bridge interfaces to surroundings. *J. Non-Equilib. Thermodyn.*, vol. 30, pp. 261 – 281.

Shevtsova, V.; Mialdun, A.; Ueno, I.; Kawamura, H.; Nishino, K.; Lappa, M. (2011): Onset of hydrothermal instability in liquid bridge. Experimental benchmark. *Fluid Dyn. Mat. Proc.*, vol. 7, pp. 1–27.

Slobozhanin, L. A.; Perales, J. M. (1993): Stability of liquid bridges between equal disks in an axial gravity field. *Phys. Fluids*, vol. 5, pp. 1305–1314.

Smith, M. (1986): Instability mechanism in dynamic thermocapillary liquid layers. *Phys. Fluids*, vol. 29, pp. 3182–3186.

Smith, M. K.; Davis, S. H. (1983): Instabilities of dynamic thermocapillary liquid layers. Part 1. Convective instabilities. *J. Fluid Mech.*, vol. 132, pp. 119–144.

Tang, Z.; Hu, W. (2005): Hydrothermal wave in a shallow liquid layer. *Microgravity Sci. Tech.*, vol. 16, pp. 253–258.

Tiwari, S.; Nishino, K. (2007): Numerical study to investigate the effect of partition block and ambient air temperature on interfacial heat transfer in liquid bridges of high prandtl number fluid. *J. Crystal Growth*, vol. 300, pp. 486 – 496.

Tiwari, S.; Nishino, K. (2010): Effect of confined and heated ambient air on onset of instability in liquid bridges of high pr fluids. *Fluid Dyn. Mat. Proc.*, vol. 6, pp. 109 – 136.

Ueno, I.; Kawazoe, A.; Enomoto, H. (2010): Effect of ambient-gas forced flow on oscillatory thermocapillary convection of half-zone liquid bridge. *Fluid Dyn. Mat. Proc.*, vol. 6, pp. 99 – 108.

Uguz, A.; Alvarez, N.; Narayanan, R. (2010): An experimental study of the stability of liquid bridges subject to shear-induced closed-flow. *J. Colloid Interf. Sci.*, vol. 346, pp. 464–469.

Wang, A.; Kamotani, Y.; Yoda, S. (2007): Oscillatory thermocapillary flow in liquid bridges of high prandtl number fluid with free surface heat gain. *Intl J. Heat Mass Transfer*, vol. 50, pp. 4195 – 4205.

Wanschura, M.; Shevtsova, V. S.; Kuhlmann, H. C.; Rath, H. J. (1995): Convective instability mechanisms in thermocapillary liquid bridges. *Phys. Fluids*, vol. 7, pp. 912–925.

Xu, J.; Zebib, A. (1998): Oscillatory two- and three-dimensional thermocapillary convection. *J. Fluid Mech.*, vol. 364, pp. 187–209.

Yura, Y.; Maruyama, K.; Nishino, K. (2009): Effects of ambient gas flow on relation between critical temperature difference and volume ratio. *JEREMI meeting–Private communication to the authors of the present article*.